Characterizing the inhibition of mammalian intestinal α-glucosidases by enantiomeric iminosugars 1,4-dideoxy-1,4-imino-L-arabinatol and 1,4-dideoxy-1,4-imino-D-arabinatol

by

Brianna Mantynen

A thesis
presented to the University of Waterloo
in fulfilment of the
thesis requirement for the degree of
Master of Science
in
Biology

Waterloo, Ontario, Canada, 2015

Author's Declaration

I hereby declare that I am the sole author of this thesis. This is a true copy of the thesis, including any required final revisions, as accepted by my examiners.

I understand that my thesis may be made electronically available to the public.

Abstract

Sucrase isomaltase (SI) and maltase glucoamylase (MGAM) are both large Family 31 glycoside hydrolases with α-glucogenic activity (Cantarel *et al*., 2009; Lombard *et al*., 2014). Mammalian SI and MGAM, expressed predominantly in the small intestine, play essential roles in the process of starch digestion. Because their activities directly control the rate of α-glucogenesis in the small intestine, they also pose a useful target for the design of α-glucosidase inhibitors, a class of drugs useful for the treatment of type 2 diabetes and other metabolic disorders.

The purpose of this work was to characterize inhibition kinetics for enantiomeric pyrrolidine iminosugars 1,4-dideoxy-1,4-imino-L-arabinatol (LAB-1) and 1,4-dideoxy-1,4-imino-D-arabinatol (DAB-1) with N- and C-terminal catalytic subunits of SI and MGAM, as well as for an additional C-terminal MGAM isoform, in the presence of three different substrates. Kinetic analysis indicates that LAB-1 is a more potent inhibitor of maltose and PNP-glucose hydrolysis than is DAB-1. Both mixed and competitive inhibition kinetics are observed for varying combinations of inhibitor, enzyme, and substrate. A general hypothesis regarding the binding of each of the two inhibitors is presented. Additionally, evidence for substrate inhibition of palatinose hydrolysis for Nt-SI and Nt-MGAM is reported and discussed.

Acknowledgements

For all the help, advice, and company, I deeply thank Marcie and Jin, and all other members of the Rose lab. Thank you to Dylan for keeping me company in the lab at odd hours last winter and for our many lively conversations about various esoteric pieces of art-music. I would like to thank the Holyoak lab members for everything they've done for me: Will, Matt, and Iain: it has been a blast.

I would also like to thank my family for supporting my (ad)venture into graduate school. Thomas, thank you for driving me to and from the lab on so many Sundays – I know you had better things to do. Thank you to Liam and Renée for our many soccer games, Saturdays spent in the garden, and storms spent on the porch. Thank you for taking my mind off of this project once in a while.

Thank you, Trevor Charles and Todd Holyoak, for being part of my committee and for encouraging and redirecting me as I moved through this project. Thank you, Professor Rob Field, for providing the compounds which made this thesis possible. Finally, thank you, David, for being such a wonderful and helpful supervisor and for teaching me so much about science from a practical perspective.

Table of Contents

List of Figures

List of Tables

List of Equations

List of Abbreviations

SI	sucrase isomaltase
MGAM	maltase glucoamylase
Ct-MGAM	C-terminal subunit of MGAM
Nt-MGAM	N-terminal subunit of MGAM
Ct-SI	C-terminal subunit of SI
Nt-SI	N-terminal subunit of SI
LAB-1	1,4-dideoxy-1,4-imino-L-arabinatol
DAB-1	1,4-dideoxy-1,4-imino-D-arabinatol
PNP-glucose	4-nitrophenyl α-D-glucopyranoside
CSID	congenital sucrase isomaltase disorder
ES	enzyme-substrate
ESI	enzyme-substrate-inhibitor
ESS	enzyme-susbtrate-substrate
EI	enzyme-inhibitor
IEI	enzyme-inhibitor-inhibitor
SDS-PAGE	sodium dodecyl sulfate polyacrylamide gel electrophoresis

Chapter 1 Introduction

1.1 Physiology and pathology of mammalian maltase glucoamylase and sucrase isomaltase

Starch digestion in mammals is mediated by a consortium of enzymes which work together to provide a series of hydrolytic activities to ultimately liberate glucose for cellular metabolism (Quezada-Calvillo *et al.*, 2007). To initiate this process, salivary and pancreatic α-amylases hydrolyze the internal α-1,4 glycosidic bonds of starch (Auricchio *et al.*, 1965; Truscheit *et al.*, 1981). A mixture of shorter branched oligomers (α-limit dextrins), linear maltooligosaccharides and maltose are liberated and become substrates for the small intestinal brush border α-glucosidases sucrase isomaltase (SI) and maltase glucoamylase (MGAM) (Auricchio *et al.*, 1965; Truscheit *et al.*, 1981). These enzymes are anchored by their N-termini to enterocytes in the mammalian small intestine (Nichols *et al.*, 2003).

SI and MGAM, two large paralogous glycoproteins (Nichols *et al.*, 2003; Naumoff, 2007), provide a spectrum of redundant and contrasting activities against the oligomeric products of starch digestion by α-amylases (Nichols *et al.*, 2009). Both human enzymes are composed of two catalytic subunits, the N- and C-termini (Quezada-Calvillo *et al.*, 2009). All four subunits exhibit catalytic activities, and all are classified as Family 31 glycoside hydrolases, based on similarity of amino acid sequences (Cantarel *et al.*, 2009; Lombard *et al.*, 2014). Characterized by their general ability to transfer the glycosyl group from a substrate to water, glycoside hydrolases may hydrolyze substrates though either a retaining (double displacement) or an inverting (single displacement) mechanism (Koshland, 1953; Sinnott, 2007). Family 31 is

comprised of retaining glycoside hydrolases, for which products of hydrolysis have the same α or β configuration as the substrate (Lombard *et al.*, 2013).

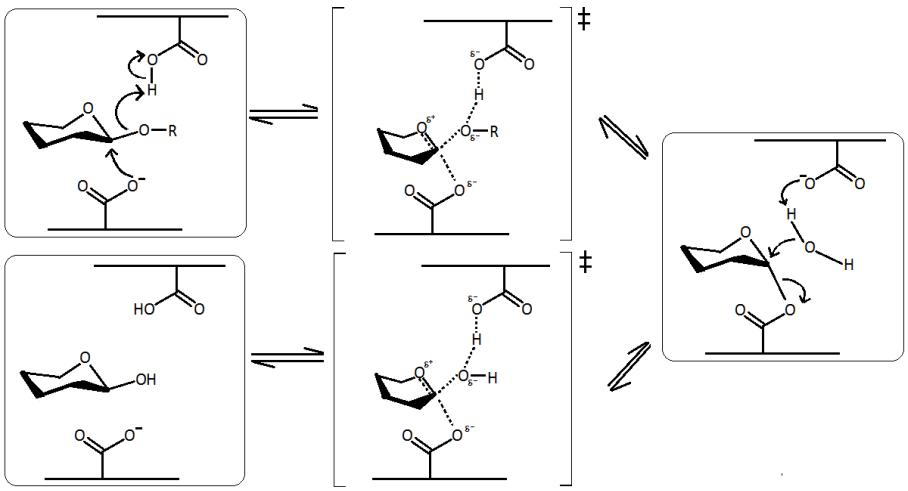

Figure 1. Retaining mechanism for glycoside hydrolases.

The retaining mechanism, proposed by Dan Koshland in 1953 (Koshland, 1953), proceeds through general acid catalysis and requires both a proton donor and a nucleophilic base (Davies and Henrissat, 1995). This double displacement mechanism involves the formation and hydrolysis of a covalent glycosyl-enzyme intermediate (McCarter and Withers, 1994). Two transition state species are formed, each a result of a separate displacement reaction (Rye and Withers, 2000).

Apparent redundancies in activities between catalytic subunits are thought to have evolved to allow for the improved digestion of many different types of starches from various botanical origins (Nichols *et al.*, 2009).

1.1.1 Physiological roles

Each of the SI and MGAM catalytic subunits has a characteristic set of substrate specificities (Jones *et al.*, 2011; Lee *et al.*, 2014). It is still not fully understood how these enzymes work together to perform the combination of hydrolytic functions required for the effective digestion of different complex carbohydrates (Lee *et al.*, 2014). Hydrolysis kinetics for a variety of substrates have, however, been well-characterized (Gray *et al.*, 1979; Jones *et al.*, 2011; Lee *et al.*, 2014; Auricchio *et al*., 1965). Albeit with differing efficiencies, all four of the subunits are able to hydrolyze the α-1,4 glycosidic linkage of maltose (Gray *et al.*, 1979; Jones *et al.*, 2011). Differences in substrate specificities provide important information about the individual roles played by each of these enzymes: the C-terminal subunit of SI, for instance, is unique in its ability to hydrolyze the α-1,2 linkage of sucrose, while the N-terminal subunit is capable of effectively hydrolysing the α-1,6 linkage of isomaltose (Gray *et al.*, 1979; Sim *et al.*, 2010). The N-terminal subunit of MGAM exhibits some isomaltase activity, but it is much less effective than the activity provided by Nt-SI (Lee *et al.*, 2014). Ct-MGAM has demonstrated no isomaltase activity at all (Lee *et al.*, 2014). It is thought that the general role of MGAM in the small intestine is to digest linear regions of oligomeric starch breakdown products, while sucrase isomaltase is responsible for the hydrolysis of branched linkages (Naumoff, 2007). The biological advantage of this spectrum of different hydrolytic activities is that it provides an organism with the capacity to derive glucose from a vast array of different complex carbohydrates (Lee *et al.*, 2014).

In addition to two catalytic subunits, both SI and MGAM also possess a transmembrane domain and an O-glycosylated stalk or "linker" region (Naumoff, 2007). The N-termini of SI

and MGAM are both located on the inside of the enterocyte membrane, while C-termini extend out into the small intestinal lumen (Semenza, 1986; Naim *et al.*, 1988). Catalytic subunits all extend into the intestinal lumen. An SI precursor protein known as Pro-SI is cleaved *in vivo* by pancreatic proteases to yield separate component subunits sucrase and isomaltase (Semenza, 1986; Naim *et al.*, 1988). After cleavage, these two catalytic subunits remain in close proximity to one another (Semenza, 1986). While potential effects of this interaction on catalytic functions of the subunits remain unclear, discrete subunits have displayed catalytic activities *in vitro* (Lee *et al.*, 2014). In contrast, maltase glucoamylase does not undergo proteolytic processing, and N- and C-terminal subunits are covalently linked (Naim *et al.*, 1988).

The gene for human sucrase isomaltase is encoded on chromosome 3q25-26 (West *et al.*, 1988), and the gene for human maltase-glucoamylase is encoded on chromosome 7q34 (Nichols *et al.*, 2003). Both SI and MGAM are considered to be the product of two ancestral duplication events (Naumoff, 2007; Nichols *et al.*, 2003). In most mammals, the C-terminal coding sequence of MGAM is composed of a series of internal tandem duplications, and different mammals exhibit different numbers of duplications (Sim, 2010). Alternative splicing of this region results in the expression of several different Ct-MGAM spliceforms, each containing different parts of the variable region (Sim, 2010). Each spliceform of Ct-MGAM possesses the glycoside hydrolase Family 31 amino acid signature sequence WIDMNE, although in different spliceforms, this sequence is located in different positions (Sim, 2010).

The spliceforms used in the present work are Ct-MGAM N2 and N20, both from mice (Sim, 2010). Interestingly, these two proteins exhibit some discrepancies in substrate specificity; for instance, Ct-MGAM N2 has been observed to have a four-fold higher affinity for maltose as

a substrate than Ct-MGAM N20 (Sim, 2010). Whether or not there are comparative differences in inhibitor potency with respect to these two spliceforms is a question of special interest.

In the present study, recombinant N-terminal subunits of SI and MGAM are human enzymes, while C-terminal subunits, Ct-SI, Ct-MGAM N2, and Ct-MGAM N20, are mouse enzymes (Sim, 2010). The amino acid sequence similarity of mouse Ct-SI and human Ct-SI is 78%, and the overall amino acid sequence similarity of mouse MGAM and human MGAM is greater than 80% (Sim, 2010). It is still fair to suppose that inferences made about human C-terminal enzymes from results observed for mouse C-terminal enzymes will be limited in scope. Although the overall architectures of these enzymes are similar, differences in amino acids present around the active site may cause the human and mouse enzymes to have quite different substrate specificities (Sim, 2010).

1.1.2 Pathology

The digestion of complex carbohydrates, including many different botanical varieties of starch, is an essential function in mammals (Quezada-Calvillo *et al.*, 2007). Unfortunately, normal digestive functions can be thwarted by a variety of genetic irregularities, including the mutation of a gene encoding an enzyme essential to this process (Jacob *et al.*, 2002). Congenital sucrase isomaltase disorder (CSID) is an example of a disease with complicated and devastating effects, caused directly by mutations to the gene encoding SI, which plays a critical role in starch metabolism (Jacob *et al*., 2002). Pathology can also develop over time in the presence of physiological abnormalities; for instance, diabetes mellitus type 2 and other metabolic disorders

involve pathological changes to the normal physiological system which disrupt regular metabolism and can lead to long-term complications and ill health (Florez, 2008).

Like many metabolic disorders, type 2 diabetes is the product of both genetic and environmental factors (Florez, 2008). It has historically been characterized as an insulin-resistant state, but it remains unclear whether the associated disease state results primarily from insulin resistance or from insufficient insulin secretion (Florez, 2008; Lillioja *et al.*, 1993; Gerich, 2000). Many long-term complications associated with type 2 diabetes are caused by hyperglycaemia, or elevated levels of plasma glucose in blood, over a long period of time (Gerich, 2000).

The disease state is highly correlated with obesity, and lifestyle factors such as diet and exercise are very important in its treatment (Gerich, 2000). Many classes of oral antidiabetic agents are also available for the treatment of type 2 diabetes, if nonpharmacological measures prove insufficient (Krentz and Bailey, 2005). Among the popular oral agents are sulphonylureas, a class of compounds which stimulate insulin secretion; biguanides, which cause decreased gluconeogenesis and reduced plasma glucose; thiazolidinediones, which activate a particular group of nuclear receptors and cause enhanced insulin sensitivity; and α-glucosidase inhibitors, which help to control the rate of digestion of carbohydrates in the small intestine (Krentz and Bailey, 2005). Proper glycaemic control is a main treatment target for this disease, and several classes of oral agents address it directly.

The α-glucosidase inhibitor acarbose, introduced onto the market in the 1990s, was the first of its class to become available for the treatment of type 2 diabetes (Krentz and Bailey, 2005). Compounds of this class bind with high affinity to α-amylases, sucrase isomaltase,

maltase glucoamylase, or a combination of these enzymes, thereby inhibiting the hydrolysis of starch, oligosaccharide and disaccharide substrates (Krentz and Bailey, 2005). This reduces the amount of monomeric glucose available for absorption along the intestinal tract (Krentz and Bailey, 2005). Larger oligomers, which would normally be hydrolyzed early on, travel further along the intestinal tract, ultimately causing the delayed absorption of glucose and circumventing the incidence of "spikes" in blood glucose, also known as postprandial hyperglycaemia (Krentz and Bailey, 2005; van de Laar *et al*., 2005). The most common adverse effects associated with antidiabetic agents of this class are gastrointestinal in nature, due to the passage of undigested oligomeric carbohydrates into the large intestine, where they become substrates for the microflora of that environment (Krentz and Bailey, 2005). This can result in abdominal discomfort, flatulence, and diarrhoea (Krentz and Bailey, 2005).

α-glucosidase inhibitors are an attractive class of oral antidiabetic agents because they are generally associated with low levels of toxicity and they do not cause weight gain (van de Laar *et al*., 2005). Since the 1990s, several new α-glucosidase inhibitors have been introduced, including miglitol and voglibose (Krentz and Bailey, 2005). *Salacia reticulata* extract, containing inhibitors of the thiosugar sulfonium sulfate class, has also been shown in one double-blind study to be an effective treatment for human patients with type 2 diabetes, with few deleterious effects (Jayawardena *et al*., 2005).

1.2 Elementary enzyme kinetics and inhibition kinetics

The first recorded observations of cell-free activity for biological samples date back to the late 1700s (Segel, 1975). Throughout the 1800s, a new idea emerged; this was the idea that cell-free activity, affecting the change of one substance into another, must be attributable to the presence of a kind of chemical catalyst (Segel, 1975). Today these chemical catalysts are known as enzymes, with almost innumerable functional roles in biological systems. Enzymes serve to decrease the activation energy required for a chemical reaction by providing an alternative mechanism to transform one or more substrates into products (Segel, 1975).

1.2.1 Unireactant steady-state kinetics for enzyme-catalyzed reactions

For the very simple case of an enzyme-catalyzed reaction with a single substrate, a single enzyme, and a single intermediate enzyme-substrate (ES) complex, the following scheme describes the reaction progress and indicates rate constants (Cornish-Bowden, 1997; Copeland, 2000). First the enzyme binds the substrate; the strength of this interaction is proportional to the magnitude of k_1, the rate constant for the formation of ES (Copeland, 2000; Stein, 2011). Dissociation of ES back to E and S is governed by the reverse rate constant, k_{-1} (Copeland, 2000). k_2 is, in the simplest case, the catalytic rate constant, and k_{-2} is the rate constant of the reverse reaction (often of negligible magnitude) (Copeland, 2000).

$$E + S \underset{k_{-1}}{\overset{k_1}{\rightleftharpoons}} ES \underset{k_{-2}}{\overset{k_2}{\rightleftharpoons}} E + P$$

Figure 2. General scheme for an enzyme-catalyzed reaction.

The rate constant k_2, describing only a simple scenario where no additional complexes are formed subsequent to formation of the ES complex, is often insufficient to describe more complex reaction mechanisms. For instance, several intermediate complexes may be formed before products are released (Segel, 1975). It is therefore necessary to describe most enzyme-catalyzed reactions using k_{cat}, a constant which governs the rate-limiting or slowest step in a series of post-ES catalytic reactions (Copeland, 2000).

In 1903, Victor Henri proposed the idea that enzyme-catalyzed reactions involved the formation of an enzyme-substrate complex at some point along the reaction coordinate (Henri, 1903). He independently derived a mathematical equation, later rediscovered and modified by the German biochemist Leonor Michaelis and by the Canadian physician Maud Menten, to describe the change in reaction velocity as a function of substrate concentration (Segel, 1975).

$$\frac{v}{V_{max}} = \frac{[S]}{K_s + [S]}$$

Equation 1. Henri-Michaelis-Menten equation for slow reaction kinetics (Segel, 1975).
where v = initial velocity (instantaneous reaction velocity, d[P]/dt or d[S]/dt)
V_{max} = maximal reaction velocity; observed when all E present has been converted to ES
[S] = substrate concentration
$K_s = k_{-1}/k_1 =$ the dissociation constant for the ES complex $\approx K_m$ when $k_2 << k_{-1}$

When the magnitude of rate constant k_2 is not negligible – that is, when slow reaction kinetics are not observed, the equation becomes

$$\frac{v}{V_{max}} = \frac{[S]}{K_m + [S]}$$

Equation 2. General Henri-Michaelis-Menten equation (Copeland, 2000).
where $K_m = (k_2 + k_{-1})/k_1$

K_m, the Michaelis constant, is distinctive for each given enzyme reacted with a given substrate (Segel, 1975). It is defined as the substrate concentration required for the instantaneous reaction velocity to reach half the magnitude of the maximal reaction velocity (Copeland, 2000). More complex kinetics, including those describing the activities of enzymes that do not follow rapid equilibrium kinetics, as well as for multireactant systems, were characterized later on in the twentieth century (Segel, 1975).

In 1913, the "steady state" concept was first described by Max Bodenstein, a German physical chemist, and was later found to be applicable to enzyme kinetics by George Briggs and J. B. S. Haldane (Segel, 1975; Stein, 2011). The essence of the steady state assumption is that any intermediate in a multistep reaction exists at a constant concentration; the rate of formation and the rate of decay are equivalent in magnitude (Stein, 2011). For a unireactant system with a single ES complex, this means that [ES] is not changing over the course of the reaction time.

Requirements of the steady state condition are listed as follows (Copeland, 2000):

- **$[S] >> [E]$**

The substrate concentration must be significantly greater than the total enzyme concentration. The amount of unbound substrate is not appreciably depleted by formation of the ES complex.

- **$[E]_t = [E] + [ES]$**

The total quantity of enzyme present does not change over the course of the reaction.

- **$[P]_o = 0$**

There are no products present at the initiation of the reaction.

Catalytic subunits of SI and MGAM, the enzymes relevant to the present work, are considered here as part of a unireactant system at steady state.

1.2.2 Linear inhibition kinetics for reversible inhibitors

Iminosugars, including LAB-1 and DAB-1, are reversible inhibitors of glycoside hydrolases (Stütz, 1999; Butters *et al*., 2005). In general, reversible inhibition can be subdivided into two categories: linear inhibition and nonlinear inhibition (Segel, 1975). Linear inhibition involves the formation of one or more nonproductive complexes resulting from a binding interaction between an inhibitor and an enzyme, or between an inhibitor and an enzyme-ligand complex (Leskovac, 2003). This type of inhibition can be further classified as competitive, noncompetitive (a form of mixed inhibition), or uncompetitive (Leskovac, 2003).

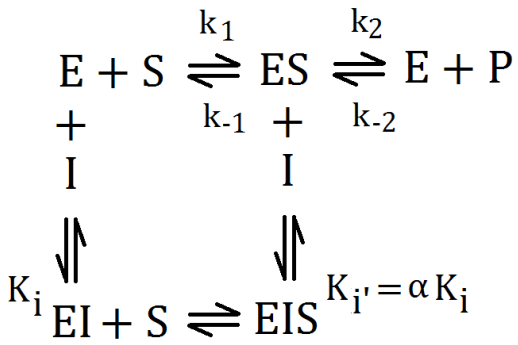

Figure 3. General scheme for linear inhibition of an enzyme-catalyzed reaction.
`where K_i represents the dissociation constant for the EI complex
K_i' represents the dissociation constant for the EIS complex
α represents the constant relating K_i and $K_{i'}$

Competitive inhibition occurs when an inhibitor binds to an enzyme's active site, thereby precluding binding of the substrate (Leskovac, 2003). The concentration of products is directly dependent on the concentration of a competitive inhibitor in solution (Segel, 1975). Henri-Michaelis-Menten kinetics are altered by the presence of a competitive inhibitor in a predictable way; the Michaelis constant, K_m, is increased (Leskovac, 2003). This is because binding of an inhibitor to the free enzyme causes a shift in chemical equilibrium which favours dissociation of the ES complex as a result of Le Châtelier's principle (Clugston and Fleming, 2000). Equation 3

describes the relationship between K_m and the apparent K_m (K_m^{app}) in the presence of a competitive inhibitor.

$$K_m{}^{app} = K_m(1 + \frac{[I]}{K_i})$$

Equation 3. Relationship between apparent K_m and actual K_m in the presence of a competitive inhibitor (Segel, 1975).

Noncompetitive inhibition refers to a type of inhibition observed when an inhibitor binds with equal preference both to the free enzyme and to the ES complex (Segel, 1975). The extent of dissociation of the two complexes formed, namely EI and EIS, is described by the magnitudes of constants K_i and $K_{i'}$, respectively. In this scenario, the inhibitor binding site is independent of the substrate binding site, and K_i and $K_{i'}$ are equal in magnitude (Segel, 1975).

$$V_{max}{}^{app} = \frac{V_{max}}{(1 + \frac{[I]}{K_{i'}})}$$

Equation 4. Relationship between apparent V_{max} and actual V_{max} in the presence of a mixed, noncompetitive, or uncompetitive inhibitor (Segel, 1975).
$V_{max}{}^{app}$ represents the observed maximal reaction velocity

Uncompetitive inhibitors bind only to the ES complex, affecting a decrease in the parameter K_m due to a shift in chemical equilibrium which must favour the formation of the ES complex (Clugston, 2000). Equation 5 illustrates the relationship between actual K_m and apparent K_m in the presence of an uncompetitive inhibitor.

Binding of an uncompetitive inhibitor also reduces the rate of catalysis, causing an equivalent decrease in V_{max} which can be described by Equation 4. Because some enzyme will always be present in the inactive ESI form, in this scenario, it is not possible to drive all of the enzyme present into the ES form, even with an infinitely high concentration of substrate (Segel, 1975).

$$K_m{}^{app} = \frac{K_m}{(1 + \frac{[I]}{K_{i'}})}$$

Equation 5. Relationship between apparent K_m and actual K_m in the presence of an uncompetitive inhibitor (Segel, 1975).

A mixed inhibitor will bind both to E and to the ES complex, with a higher affinity for one form than for the other, causing K_i and $K_{i'}$ to be of different magnitudes (Segel, 1975). Both the Michaelis constant and the maximal reaction velocity will be affected by the binding of this class of inhibitor; the extents to which they are affected will differ, however. The change in K_m observed as a result of the binding of a mixed inhibitor is illustrated in Equation 6. As can be seen from Equation 4, the apparent V_{max} is decreased in the presence of this type of inhibitor.

$$K_m{}^{app} = K_m \frac{(1 + \frac{[I]}{K_i})}{(1 + \frac{[I]}{K_{i'}})}$$

Equation 6. Relationship between apparent K_m and actual K_m in the presence of a mixed inhibitor (Segel, 1975).

Linear mixed inhibition can result from several different situations. It may be the result of an inhibitor binding to a single site and altering the affinity the enzyme has for its substrate, as well as the enzyme's ability to effectively catalyze the reaction (Segel, 1975). This type of inhibition may also result when an inhibitor binds at two distinct sites on the enzyme (Segel, 1975). In the latter case, binding of one inhibitor molecule must obstruct binding of the substrate, and while binding at the second site has no effect on substrate binding, it does produce a catalytically inactive ESI complex (Segel, 1975). In some cases, IEI complexes can form if inhibitor binding events at two sites are not mutually exclusive (Segel, 1975).

1.2.3 Nonlinear inhibition kinetics for reversible inhibitors

Nonlinear inhibition kinetics in monosubstrate reactions may result from several different phenomena (Leskovac, 2003). One case of nonlinear inhibition kinetics is when a productive ESI complex forms (Segel, 1975; Whitely, 1997). This phenomenon is governed by hyperbolic inhibition kinetics, named for the character of the secondary replots which distinguish them from linear or parabolic inhibition kinetics (Leskovac, 2003). When the ESI complex can yield products with no loss of catalytic activity, the system demonstrates hyperbolic competitive inhibition kinetics (Segel, 1975). Hyperbolic mixed inhibition is also possible: in this case, both

the ES complex and the ESI complex can yield products, but the ESI complex has decreased catalytic activity and therefore cannot render products as effectively (Segel, 1975). Hyperbolic noncompetitive and hyperbolic uncompetitive inhibition systems are similar to their linear counterparts, with the sole difference being development of products from an ESI complex (Leskovac, 2003). Indeed, all instances of hyperbolic inhibition are partial in nature, and a saturating concentration of inhibitor cannot completely quench the reaction; some enzyme will always be present in the EIS form, rendering products (Leskovac, 2003).

Nonlinear inhibition kinetics may also be the result of multiple inhibitor binding events – this is referred to as parabolic inhibition (Leskovac, 2003). Parabolic inhibition is considered a type of complete inhibition, because under conditions of saturating [I], all enzyme present will be driven to an inactive form, IEI (Leskovac, 2003).

1.3 A review of iminosugar inhibitors and thiosugar sulfonium salts

In the discovery and development of candidate inhibitors of mammalian α-glucosidases, iminosugars and thiosugar sulfonium salts have been among the most rigorously researched classes of compounds (de Melo *et al*., 2006). The isolation of naturally-occurring compounds such as nojirimycin, from *Streptomyces sp.* (Ishida *et al*., 1967), and salacinol, from *Salacia reticulata* (Yoshikawa *et al*., 1997), instigated a hunt for similar natural compounds and informed the rational design of biologically-active derivatives. The following sections will provide a review of the structural differences and biological activities of piperidine and pyrrolidine iminosugar inhibitors. Structural differences and biological activities of thiosugar sulfonium sulfates will be reviewed thereafter.

1.3.1 Piperidine and pyrrolidine iminosugars

Both naturally-occurring and synthetically-derived iminosugars have been well-characterized as inhibitors of an impressive variety of enzymes, including but not limited to α- and β-glucosidases, glycosyl transferases, phosphorylases, sugar-nucleotide mutases, and glycogen phosphorylases (Rule *et al*., 1985; Fleet *et al*., 1985; Evans *et al.*, 1985; Scofield *et al*., 1986; de Melo *et al*., 2006; Andersen *et al*., 1999). Inhibitors of this class have been most actively studied for their often potent effects on α-glucogenic activities (Asano, 2003). For this reason, iminosugar inhibitors have long been of interest as potential antidiabetic agents.

1.3.1.1 Iminosugars: Structural Characteristics and Mechanisms of Inhibition

Iminosugars are generally classified by the nature of the ring structures of which they are composed. Monocyclic iminosugars include pyrrolidines, which resemble furanose rings, and piperidines, which resemble pyranose rings (Asano *et al*., 2005). Many bicyclic alkaloid structures, including indolizidines, pyrrolizidines, and nortropanes, have also been identified as glycosidase inhibitors (de Melo *et al*., 2006; Asano *et al*., 2000; Molyneux *et al*., 2002).

The piperidine iminosugar nojirimycin (NJ), originally isolated in 1966 as an antibiotic from *Streptomyces roseochromogenes* (Ishida *et al*., 1967), has been identified as an inhibitor of both α- and β-glucosidic activities (de Melo *et al*., 2006; Asano *et al*., 2000). Like other piperidine iminosugars, NJ is a six-membered heterocyclic compound containing endocyclic nitrogen (Asano *et al*., 2000). Well-studied NJ derivatives include 1-deoxynojirimycin (DNJ) and deoxygalactonojirimycin (DGJ) (Asano *et al*., 2000).

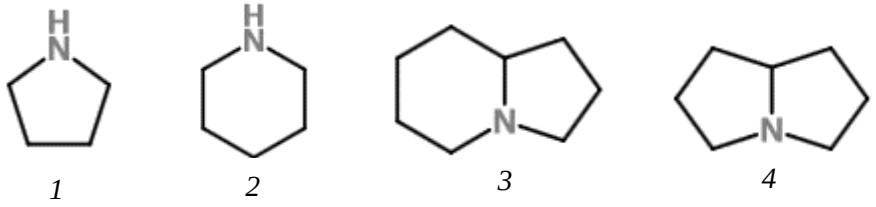

Figure 4. Basic chemical structures of four classes of iminosugar inhibitors: *1*, pyrrolidines, *2*, piperidines, *3*, indolizidines, and *4*, pyrrolizidines.

Pyrrolidine and piperidine iminosugars, including NJ, have frequently been described as substrate mimics, and ostensibly influence substrate binding by means of competition for an enzyme's active site (de Melo *et al*., 2006; Asano *et al*., 2000). There exist several hypotheses

about the general mechanism by which iminosugars exert inhibitory effects, but they are all based on the fundamental concept of structural mimicry (de Melo *et al*., 2006; Asano *et al*., 2005). Many iminosugars are highly effective inhibitors of glycosidases, and it is widely accepted that this is generally because they structurally mimic either a unit of a natural substrate or a transition state species (de Melo *et al*., 2006; Asano *et al*., 2005).

The transition state species in a glycosidic cleavage reaction is considered the molecular structure with the highest potential energy along the reaction coordinate (Nash *et al*., 1965; Ozaki *et al*., 2008). This species requires enzymatic stabilisation in order for the reaction to proceed toward products (Nash *et al*., 1965). Enzymes are evolved to very effectively stabilise transition state species so that they can perform highly specific functions (Nash *et al*., 1965). For this reason, enzymes generally have very high affinities for molecules which are structurally similar to the transition state species of a natural biological reaction.

1.3.1.2 Iminosugars: Biological Activities

The inhibitory capacity of a pyrrolidine iminosugar of special interest, 1,4-dideoxy-1,4-imino-D-arabinatol (DAB-1), was first characterized in 1985 by George Fleet and Paul Smith at Oxford University (Fleet *et al*., 1985). Here, DAB-1 was identified as a competitive inhibitor of α-glucosidic activity from Brewer's yeast (Fleet *et al*., 1985). Fleet and Smith also showed that DAB-1 was identical to a naturally-occurring compound previously isolated from *Arachniodes standishii* (Furukawa, 1985) and *Angylocalyx boutiqueanus* (Fleet *et al.*, 1985; Nash *et* al., 1985). At this time, Fleet and Smith reported that the L-enantiomer, LAB-1, was a significantly weaker inhibitor of α-glucosidic activity from Brewer's yeast (Fleet *et al.*, 1985).

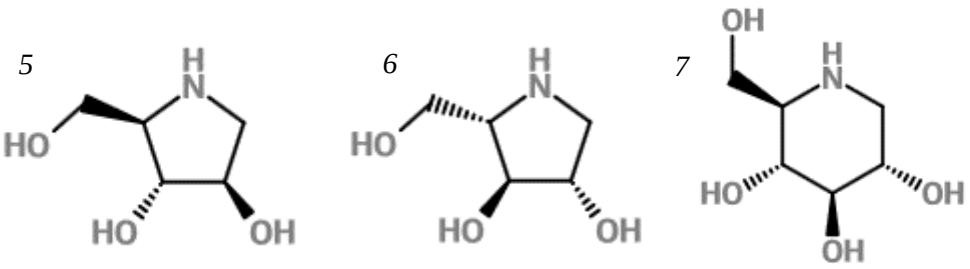

Figure 5. Chemical structures of iminosugar inhibitors *5*, DAB-1, *6*, LAB-1, and *7*, DNJ.

In 1986, George Fleet and colleagues assayed the enantiomers LAB-1 and DAB-1 for inhibition of maltase and isomaltase activities of a mouse intestinal mucosal suspension (Scofield *et al*., 1986). This series of experiments yielded an interesting result: in contrast to the relative inhibitory effects of LAB-1 and DAB-1 observed when tested with Brewer's yeast α-glucosidase, against mammalian α-D-glucosidase activity, LAB-1 was found to have a potency of an order of magnitude greater than DAB-1 (Scofield *et al*., 1986). It was concluded that the synthetic iminosugar LAB-1 was a more potent inhibitor of mammalian intestinal disaccharidase activity than was its D-enantiomer (Scofield *et al*., 1986). Because purified recombinant mammalian intestinal α-glucosidases were unavailable at the time, it was not a practical possibility in 1986 to determine precise modes of inhibition associated with DAB-1 and LAB-1 (Scofield *et al*., 1986). Nonetheless, the relative potencies of these L-and D-enantiomers of pyrrolidine iminosugars, with respect to mammalian α-glucosidase activity, demonstrated the relevance of their structural differences and suggested the potential for heterogeneity in the compounds' modes of inhibition (Scofield *et al*., 1986). It has long been a subject in need of clarification.

Since the early pioneering works of George Fleet and colleagues, differential inhibition by L- and D-enantiomers of polyhydroxy iminosugars has remained a subject of academic interest. In 2005, three pairs of iminosugar enantiomers were assayed for inhibition of a considerable

number of enzymes, including α- and β-D-glucosidases, α- and β-D-mannosidases, α- and β-D-galactosidases, and amyloglucosidase, from a number of different organisms (Asano *et al*., 2005). Iminosugars tested included LAB-1 and DAB-1, L- and D- isofagomine (piperidine iminosugars), and L- and D-DMDP (2,5-dideoxy-2,5-imino-mannitol; pyrrolidine imminosugars) (Asano *et al*., 2005). This investigation showed that the three D-enantiomers inhibited both yeast and rat α-D-glucosidase activity in a purely competitive manner, while L-enantiomers exhibited purely non-competitive inhibition against the same enzymes (Asano *et al*., 2005). These results provoked the question of whether LAB-1 and DAB-1 were binding to the same site, or whether LAB-1 bound to a remote allosteric site (Asano *et al*., 2005). The matter has not been definitively settled.

A recent study investigated the inhibition of rat α-D-glucosidic activities by N-benzyl derivatives of pyrrolidine iminosugars (Carreiro *et al*., 2014). Analysis of inhibition kinetics for N-benzylated compounds revealed several instances of weak mixed inhibition (Carreiro *et al*., 2014). Since iminosugar inhibitors commonly exhibit competitive inhibition kinetics (Krasikov *et al*., 2001), structural modifications that influence an inhibitor's effects on substrate affinity and enzymatic catalysis may provide useful information for rational drug design.

A central weakness of iminosugar inhibitors as a group is that many compounds are somewhat nonselective and exert diverse biological effects by interacting with an assortment of enzymes (Asano *et al*., 2005). Interestingly, several iminosugars including LAB-1, castanospermine, and a host of DNJ derivatives, have demonstrated anti-HIV activities *in vitro* (Fleet *et al*., 1988; Greimel *et al*., 2003), and castanospermine specifically has been implicated in the blockage of mouse tumour cell metastasis via inhibition of glucosidase I, an enzyme which initiates the processing of N-linked glycoproteins (Humphries *et al*., 1986). The fact that iminosugars demonstrate such a great variety of interactions makes them attractive as first-

generation compounds for drug development while simultaneously decreasing their direct use in the treatment of metabolic disorders and disease (Horne *et al.*, 2011).

1.3.2 Thiosugar sulfonium sulfates

Investigation of thiosugar sulfonium sulfates began in 1990, when a research group from Toyama, Japan characterized the effects of an aqueous *Salacia reticulata* extract on plasma glucose levels in streptozotocin-induced diabetic rats (Serasinghe *et al.*, 1990). *Salacia reticulata* has been used traditionally in the Ayurvedic system of Indian Medicine to treat diabetes (Yoshikawa *et al*., 1997). Biochemical investigations of oral hypoglycaemic activity of aqueous extracts from *S. reticulata* root bark were first reported in 1997, when Masayuki Yoshikawa *et al.* described the thiosugar sulfonium sulfate structure of the antidiabetic agent salacinol (Yoshikawa *et al*., 1997). This initiated a wave of investigations into the effects of other thiosugar sulfonium sulfates present in *S. reticulata* extracts, as well as synthetically-produced derivatives.

As a result, another yet more potent antidiabetic principle was isolated from aqueous *S. reticulata* extract; this compound, called kotalanol, differed from salacinol only by the nature of the side chain extending off of the ring sulfur atom (Yoshikawa *et al*., 1998). The sulfate group present on the side chain of kotalanol is oriented slightly differently in space, and the side chain itself is seven carbon atoms in length, while the side chain of salacinol is only four carbon atoms in length (Yoshikawa *et al*., 1997; Yoshikawa *et al*., 1998). The significance of stereochemistry of the hydroxyl groups located at different positions on the kotalanol side chain would not be demonstrated before nearly a decade had passed (Tanabe *et al*., 2012). In the meantime, side chain analogues ponkoranol and salaprinol (Yoshikawa *et al*., 2008) and de-O-sulfonated

analogues (Minami *et al.*, 2008; Ozaki *et al*., 2008; Muraoka *et al*., 2008)) were isolated and characterized in a series of different ventures.

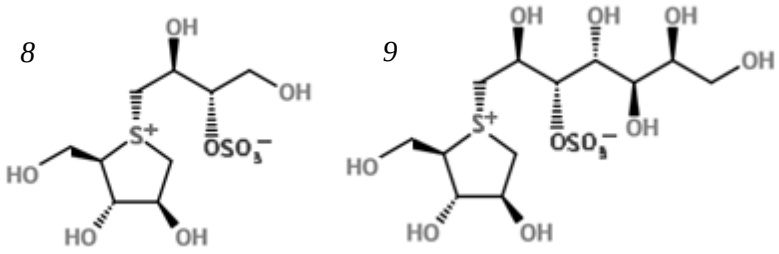

Figure 6. Chemical structures of two compounds isolated from *Salacia reticulata*: salacinol (*9*) and kotalanol (*9*).

1.3.2.1 Thiosugar sulfonium sulfates: Structural Characteristics and Mechanisms of Inhibition

Structurally, thiosugar sulfonium salts bear some similarities to the pyrrolidine iminosugars relevant to the present investigation; the five-membered rings of salacinol and kotalanol resemble the furanose-like ring of DAB-1 with respect to hydroxyl group stereochemistry, but include sulfur as the ring heteroatom instead of nitrogen (Yoshikawa *et al*., 1997; Yoshikawa *et al*., 1998; Yoshikawa *et al*., 2002). Structural characteristics such as ring hydroxyl group stereochemistry (Mohan and Pinto, 2007), the nature of the ring heteroatom (Gallienne *et al.*, 2006; Mohan and Pinto, 2007), side chain stereochemistry (Tanabe *et al.*, 2012; Mohan and Pinto, 2007), variation of chiral centers (Gallienne *et al*., 2006), and variation of ring size (Gallienne *et al.*, 2006) all play an important role in determining the potency of thiosugar sulfonium sulfates and related inhibitors.

Thiosugar sulfonium sulfates have distinctive zwitterionic structures, relying on stablilization of the ring sulfonium cation by a sulfate anion provided by the side chain

(Gallienne *et al*., 2006; Mohan and Pinto, 2007; Lillelund *et al*., 2007). It is thought that salacinol exerts inhibitory effects by mimicking an oxocarbenium-ion-like transition state species in the hydrolysis of natural polysaccharide or glycoside substrates (Gallienne *et al*., 2006). There is great variability in potency associated with this class of inhibitors, with respect to different glycosidases of different origins (Yuasa *et al*., 2001). For these inhibitors, it is purported that potency with respect to different enzymes is directly related to how accurately the structure of the inhibitor mimics the structure of an oxocarbenium-ion-like transition state (Stötz, 1999). As is the case with the iminosugar inhibitors, the ring heteroatom of this class of inhibitors is thought to provide a positive charge to mimic the partial positive charge on the endocyclic oxygen atom of a transition state (Stötz, 1999).

There is ample evidence that electrostatic interactions also play an important role in the determination of the potencies of different thiosugar sulfonium sulfate inhibitors (Stötz, 1999; Ghavami *et al*., 2001). Structural modifications which exploit hydrogen bonding phenomena via altered hydroxyl group stereochemistry, or which exploit electrostatic and hydrophobic interactions, are therefore key to the development of successful inhibitors.

1.3.2.2 Thiosugar sulfonium sulfates: Biological Activities

Naturally-occurring compounds isolated from *S. reticulata* (Yoshikawa *et al*,, 1997; Yoshikawa *et al*., 1998; Ozaki *et al*., 2008) and related species including *S. prinoides* (Yoshikawa *et al*., 2008) are thought to be a by-product of coevolution between plants and the herbivores and omnivores that consume them (Marles and Farnsworth, 1995). These hypoglycaemic agents are generally considered chemical defense compounds evolved by plants to deter predators (Marles and Farnsworth, 1995). Since it is advantageous for plants to produce

chemicals which can affect a broad range of predators, active compounds isolated from a natural source often exhibit poor selectivity (Marles and Farnsworth, 1995). This may explain why structures of naturally-occurring iminosugars and thiosugar sulfonium sulfates are such that they inhibit the functions of a variety of different enzymes.

Salacinol analogues have shown inhibitory activities against mammalian α-glucosidases (Jones *et al*., 2011) and against a *Drosophila* homologue of human Golgi α-mannosidase II (Kuntz *et al*., 2005), and certain derivatives have demonstrated activities against β-glucosidases (Gallienne *et al.*, 2005) and β-galactosidases (Gallienne *et al*., 2006). Several analogues exhibit the capacity to bind to more than one target enzyme (Jones *et al*., 2011; Kuntz *et al*., 2005). If a compound is intended as a candidate drug for the treatment of a metabolic disorder, it is essential that the compound does not interact non-selectively with a broad range of enzymes present in the human body. In order to improve the selectivity of these compounds, it is necessary to examine the precise effects that controlled structural modifications have on inhibition kinetics. Even apparently minor changes to an inhibitor's structure can dramatically alter its selectivity (Gallienne *et al*., 2006).

Salacinol and kotalanol exhibit classic competitive inhibition kinetics with recombinant subunits of both human maltase glucoamylase and sucrase isomaltase (Rossi *et al*., 2006; Sim, 2010; Sim *et al*., 2010; Jones *et al*., 2011). For maltose hydrolysis reactions in the presence of salacinol and kotalanol, inhibition constants are all in the low micromolar or nanomolar range (Jones *et al*., 2011). The incidence of differential competitive inhibition of recombinant SI and MGAM subunits reinforces the notion that the active site architectures for each of these enzymes have evolved to perform a characteristic set of functions. The competitive inhibition associated with this class of compounds indicates that they bind in the active site of affected enzymes,

thereby impeding substrate binding (Sim *et al*., 2010). In 2008, a crystal structure of Nt-MGAM was reported in complex with acarbose (Sim *et al*,, 2008), and in 2010, the same group obtained the crystal structure of Nt-SI in complex with kotalanol (Sim *et al*., 2010). Both inhibitors were found in the active sites of the respective structure (Sim *et al*., 2010). These reports laid the groundwork for the development of inhibitors that might be tailored to the unique active site features of the different mammalian small intestinal α-glucosidases.

1.4 Thesis Objectives

The value of characterizing inhibition kinetics for compounds with inhibitory activities against mammalian digestive α-glucosidases is twofold. Firstly, such research can elucidate the various mechanisms by which inhibitors and enzymes interact; it can also serve to clarify how or if the structures of different substrates affect this relationship. Secondly, it may provide information about structural characteristics of enzyme active sites – information that may prove invaluable in the hunt for potent and highly selective α-glucosidase inhibitors.

The second chapter of this thesis will describe assays performed for the purpose of characterizing inhibition kinetics of LAB-1 and DAB-1 with five different intestinal α-glucosidases and the disaccharide maltose, which is composed of glucose units connected by an α-1,4 glycosidic linkage. Chapter 2 will also outline the execution of another type of assay, one for which 4-nitrophenyl-α-D-glucopyranoside (PNP-glucose) was used as the substrate.

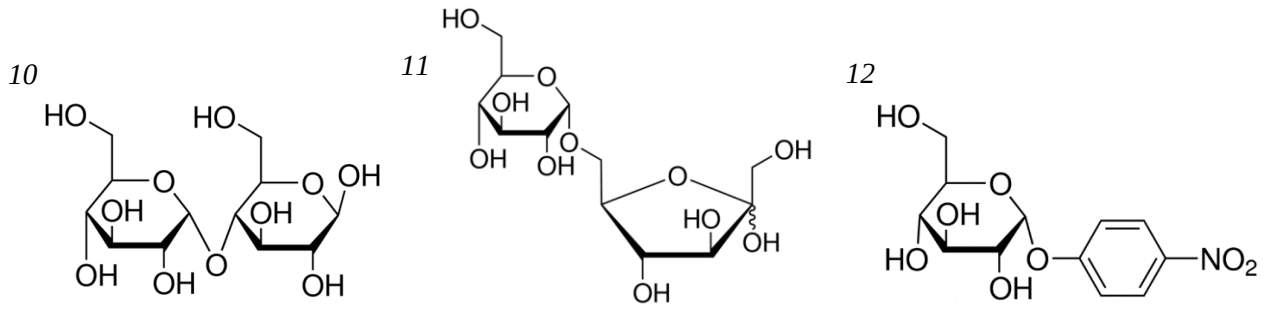

Figure 7. Chemical structures of maltose (*10*), palatinose (*11*), and PNP-glucose (*12*).
Images adapted from http://www.sigmaaldrich.com.

The ultimate purpose of this work is to provide a detailed analysis of inhibition of mammalian small intestinal α-glucosidases by the polyhydroxylated pyrrolidine inhibitors LAB-1 and DAB-1. By using purified recombinant SI and MGAM subunits, it is possible to more precisely describe the mechanisms by which these two inhibitors exert their effects. This information will contribute to our scientific understanding of pyrrolidine iminosugars and their roles as α-glucosidase inhibitors.

Chapter 2 Materials and Methods

2.1 Assays for inhibition of maltose hydrolysis

Unless otherwise indicated, all chemicals were sourced from Sigma-Aldrich.

Each assay for maltase activity was performed in two 96-well microtitre plates, adapted from the method of Arne Dahlqvist (Dahlqvist, 1961). Completion of the assay depended on several sequential reactions: an initial hydrolysis reaction, and a subsequent series of reactions for development of a secondary chromophoric product. The assay's first step involved the hydrolytic cleavage of maltose to two glucose molecules in the presence of MGAM or SI. This reaction is represented by Equation 7.

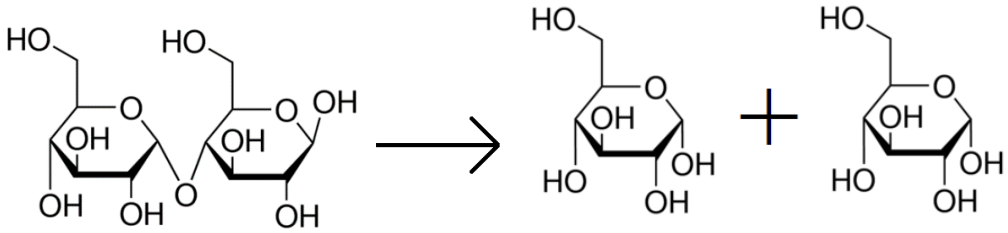

Equation 7. Hydrolysis of maltose by MGAM or SI.
Images adapted from http://www.sigmaaldrich.com.

Before addition to the reaction mixture, maltose was dissolved in a buffer containing 200 mM MES monohydrate at pH 6.5. The reaction was immediately incubated at 37°C, and had a final reaction volume of 50 µL. The reaction time was 45 minutes. Enzyme stocks contained 10 mM NaCl and 20 mM Tris, at pH 8; stocks were highly diluted (1:100 to 1:500) with Milli-Q™ water before use in assays. Variable quantities of each recombinant subunit were added; these quantities are recorded in Table 1. Any inhibitors added to the reaction were dissolved in 200

mM MES monohydrate, pH 6.5. The total reaction volume was divided up as follows: 10 µL enzyme, 10 µL inhibitor, and 30 µL substrate.

Table 1. Enzyme quantities used in assays for inhibition of maltase activity.

Catalytic Subunit	Quantity Added to Reaction (ng)
Nt-SI	6.7
Ct-SI	5.0
Nt-MGAM	10
Ct-MGAM N2	2.0
Ct-MGAM N20	6.7

The range of substrate concentrations tested in each assay was tailored to each catalytic subunit; ideal ranges were determined by trial and error. This was done to ensure fair representation of both linear and plateau regions of Michaelis-Menten curves and to improve estimates of kinetic parameters K_m (mM) and V_{max} ($molL^{-1}s^{-1}$). Inhibitor concentration ranges were also adjusted to improve resolution of inhibitory effects; ranges spanned from 15-200 nM to 1.2-8 µM, depending on which enzyme-substrate pair was used.

Upon completion of the first incubation period, assay microplates were removed to room temperature. The first reaction was quenched using 25 µL of a buffer containing 3M Tris, pH 6.9. A mixture of reduced o-dianisidine and the enzyme glucose oxidase-peroxidase (Dahlqvist, 1961), with a total volume of 125 µL, was added to initiate the second reaction, described by Equation 8. Microplates were immediately incubated at 37 degrees Celsius.

$$\text{Glucose} + H_2O + O_2 \rightarrow \text{D-Gluconic Acid} + H_2O_2$$

Equation 8. Oxidation of glucose by glucose oxidase-peroxidase.

Formation of H_2O_2 allowed another reaction to take place: H_2O_2 oxidized the reduced o-dianisidine to form oxidized o-dianisidine, a brown-coloured product detectable by spectrophotometer at 450 nm. On the same microplates used for the assay, a glucose standard curve was included and used to calculate glucose liberated over the total reaction time of 45 minutes. Quadruplicate absorbance values for each data point were used to determine glucose concentrations, and ultimately initial velocities for hydrolysis of maltose. In this series of experiments, the rate was defined as $molL^{-1}s^{-1}$ of glucose developed over the course of the reaction. Accounting for the stoichiometry of maltose hydrolysis, the real rate of the reaction was considered one-half of the rate of total glucose production.

$$H_2O_2 + \text{Reduced o-dianisidine} \rightarrow \text{Oxidized o-dianisidine}$$

Equation 9. Reaction of reduced o-dianisidine with hydrogen peroxide.

All five enzymes, Nt-SI, Ct-SI, Nt-MGAM, Ct-MGAM N2, and Ct-MGAM N20, were tested in separate assays with the inhibitors LAB-1 and DAB-1. The thiosugar sulfonium sulfate inhibitor salacinol was used as a positive control for inhibition of maltase activity. No blank rate was observed over the range of maltose concentrations used in this assay.

2.2 Assays for palatinose hydrolysis

Assays involving palatinose as a substrate were performed following nearly identical methods to those described for maltase activity assays. Methods that deviated from the maltase activity assay protocol are described as follows:

- Hydrolysis of palatinose liberates one glucose molecule, as indicated in Equation 10. When initial rates were calculated form absorbance data, this stoichiometry was taken into account.

$$\text{Palatinose} \rightarrow \text{Glucose} + \text{Fructose}$$

Equation 10. Hydrolysis of palatinose by MGAM or SI.

- Enzyme quantities used in this series of assays are recorded in Table 2.

Table 2. Enzyme quantities used in assays for inhibition of palatinose hydrolysis.

Catalytic Subunit	Quantity Added to Reaction (ng)
Nt-SI	67
Nt-MGAM	200

**C-terminal isoforms were not found to have any ability to hydrolyze palatinose.*

- A blank rate was observed for a negative control trial lacking enzyme. This was presumed to be caused by a small amount of glucose contaminating the substrate, since the rate of glucose measured at the assay end point was directly proportional to the concentration of palatinose in solution. The blank rate was characterized and subtracted from rate data for all assays with palatinose as the substrate.

2.3 Assays for inhibition of PNP-glucose hydrolysis

Assays with PNP-glucose involved only one reaction, since hydrolysis of this substrate produces equimolar amounts of glucose and nitrophenol. PNP-glucose was dissolved in 200 mM MES monohydrate at pH 6.5. Once again, substrate and inhibitor concentration ranges were tailored to individual enzymes for optimal representation and resolution of Michaelis-Menten plots. Due to substrate solubility limitations, the maximum effective concentration of PNP-glucose used in these assays was 30 mM.

Importantly, only the deprotonated nitrophenolate ion is chromophoric, so upon completion of a 45-minute incubation period, the reaction was stopped and alkaline conditions were introduced via the addition of 150 µL of 500 mM sodium bicarbonate buffer, pH 10. Microplates were read by spectrophotometer at 405 nm.

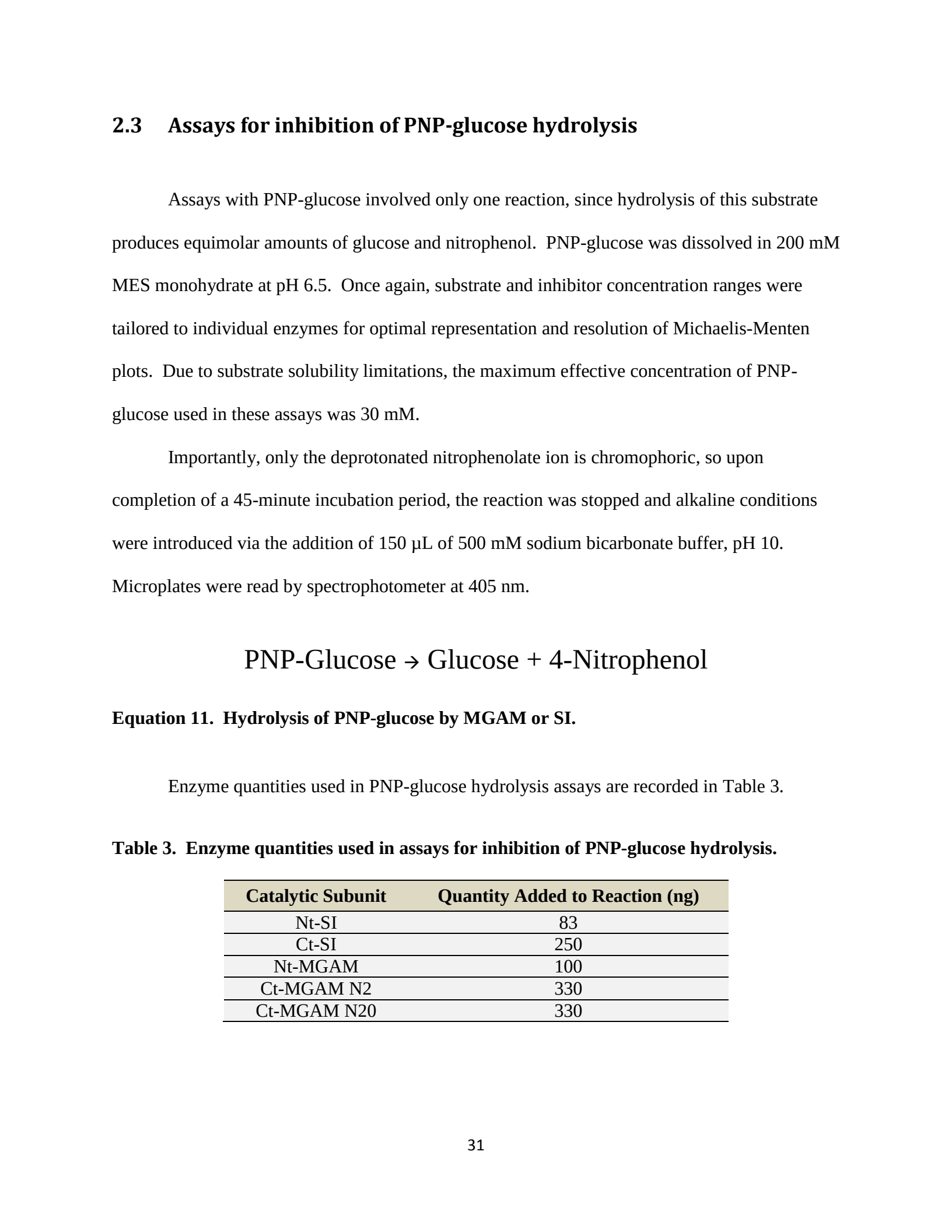

Equation 11. Hydrolysis of PNP-glucose by MGAM or SI.

Enzyme quantities used in PNP-glucose hydrolysis assays are recorded in Table 3.

Table 3. Enzyme quantities used in assays for inhibition of PNP-glucose hydrolysis.

Catalytic Subunit	Quantity Added to Reaction (ng)
Nt-SI	83
Ct-SI	250
Nt-MGAM	100
Ct-MGAM N2	330
Ct-MGAM N20	330

2.4 Nickel column purification of Ct-MGAM N2 and N20

Purification of Ct-MGAM N20 and Ct-MGAM N2 was performed by affinity chromatography using a nickel-NTA column. Methods for purification of these two proteins were identical. Ct-MGAM subunits were expressed individually from Baculovirus constructs in High Five insect cells at the Baylor College of Medicine in Houston, Texas. C-terminal His-tagged Ct-MGAM was secreted from insect cells into liquid media. Media was centrifuged for 30 minutes at 9000 RPM and the supernatant, containing secreted soluble proteins, was decanted into a sterile flask. After this, the supernatant was vacuum-filtered through a 500 mL Rapid-Flow™ filter unit with a 0.1 μm aPES membrane. The supernatant underwent overnight batch binding with HisPur™ Ni-NTA resin from ThermoScientific, Inc. (4 mL of resin per 500 mL of media). Resin had been previously equilibrated using a buffer containing 300 mM NaCl and 50 mM NaH_2PO_4, pH 8. No imidazole was included during batch binding. The resin was subsequently washed with two resin bed volumes of a buffer containing 10 mM imidazole, 300 mM NaCl, and 50 mM NaH_2PO_4, pH 8. A series of buffers containing increasing concentrations of imidazole (25 mM to 500 mM) were used to elute the target protein from a BioRad column, 2.5 cm in diameter.

Elutions containing Ct-MGAM N2 or N20 were concentrated to a volume of 5 mL using a 50K Amicon® Ultra centrifugal filter unit. Next, the sample was subjected to a buffer exchange using 50K Amicon® Ultra microcentrifuge filter unit. Protein was exchanged into a buffer containing 10 mM NaCl and 20 mM Tris, pH 8 and stored at -80 degrees Celsius.

Ct-SI, Nt-SI, and Nt-MGAM preparations used in the present inhibition assays were all purified at an earlier date by Kyra Jones. MGAM preparations are shown in Figure 8.

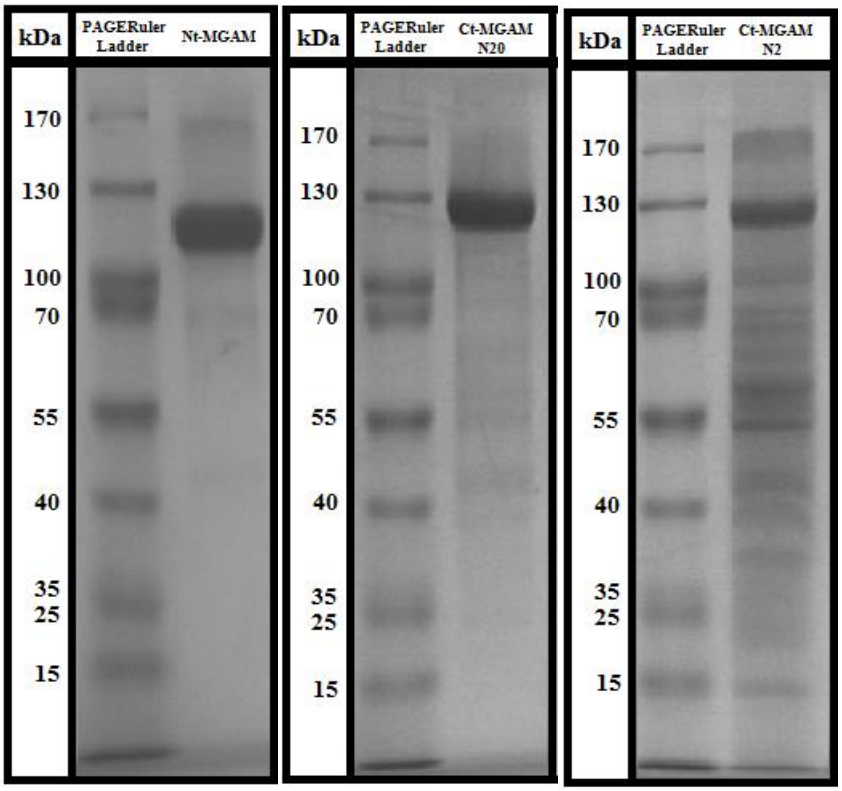

Figure 8. MGAM preparations used for inhibition assays (14% denaturing gel)

**Nt-MGAM was purified by Kyra Jones*

*** All assays with Ct-MGAM N2, except for the assay involving DAB-1 and PNP-glucose, were performed using the preparation indicated here. The second preparation is indicated in Appendix I.*

Figure 9 contains SDS-PAGE photos for SI preparations.

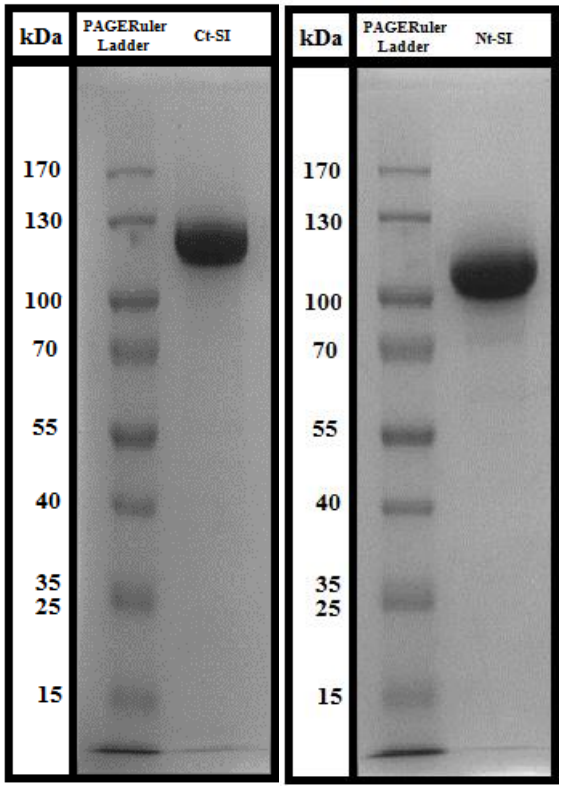

Figure 9. SI preparations used for inhibition assays (14% denaturing gel)
**Both Ct-SI and Nt-SI were purified by Kyra Jones*

2.5 Inhibition assay data analysis

Nonlinear curve fitting for substrate inhibition plots was performed using KaleidaGraph™ software from Synergy Software; curves were fit using the Levenberg-Marquardt algorithm (a Damped Least Squares method). All inhibition assay data analysis was performed using the SigmaPlot Version 13.0 Enzyme Kinetics module (Systat Software, San Jose, CA). When global curve fitting did not yield sufficiently unambiguous results, local curve analyses were performed using KaleidaGraph™ software.

Rate equations for full and partial competitive, noncompetitive, and mixed inhibition systems are included on the following page.

Equations 12-17 (Segel, 1975):

Full Competitive:

$$\frac{v}{V_{max}} = \frac{[S]}{K_m\left(1+\frac{[I]}{K_i}\right)+[S]}$$

Full Noncompetitive:

$$\frac{v}{V_{max}} = \frac{[S]}{K_m\left(1+\frac{[I]}{K_i}\right)+[S]\left(1+\frac{[I]}{K_i}\right)}$$

Full Mixed-type:

$$\frac{v}{V_{max}} = \frac{[S]}{K_m\left(1+\frac{[I]}{K_i}\right)+[S]\left(1+\frac{[I]}{\alpha K_i}\right)}$$

Partial Competitive:

$$\frac{v}{V_{max}} = \frac{[S]}{K_m\frac{(1+\frac{[I]}{K_i})}{(1+\frac{[I]}{\alpha K_i})}+[S]}$$

Partial Noncompetitive:

$$\frac{v}{V_{max}} = \frac{[S]}{K_m\frac{(1+\frac{[I]}{K_i})}{(1+\frac{\beta[I]}{K_i})}+[S]\frac{(1+\frac{[I]}{K_i})}{(1+\frac{\beta[I]}{K_i})}}$$

Partial Mixed-type:

$$\frac{v}{V_{max}} = \frac{[S]}{K_m\frac{(1+\frac{[I]}{K_i})}{(1+\frac{\beta[I]}{\alpha K_i})}+[S]\frac{(1+\frac{[I]}{\alpha K_i})}{(1+\frac{\beta[I]}{\alpha K_i})}}$$

Chapter 3 Results and Discussion

3.1 Kinetic parameters for hydrolysis of maltose, palatinose, and PNP-glucose

Replicates of all hydrolysis assays were performed with no inhibitor present in order to establish Michaelis constants for different enzyme-substrate combinations. K_m values were determined and compared with literature values where possible.

3.1.1 Kinetic parameters for hydrolysis of maltose and PNP-glucose

Kinetic parameters for hydrolysis of maltose and PNP-glucose were obtained by nonlinear regression of rate data from spectrophotometric experiments using KaleidaGraph™ software. Table 4 illustrates K_m, k_{cat}, and k_{cat}/K_m values obtained from maltose hydrolysis assays with no inhibitor present.

Table 4. Kinetic parameters for α-glucosidases with maltose substrate

†Enzyme-Substrate Pair	K_m (mM) ‡	k_{cat} (s^{-1}) ‡	k_{cat}/K_m ($s^{-1}mM^{-1}$)
[7] Nt-SI & Maltose	6.58 +/- 0.76	26.8 +/- 3.7	4.1
[13] Ct-SI & Maltose	5.42 +/- 0.20	24.9 +/- 2.1	4.6
[7] Ct-MGAM N2 & Maltose	0.858 +/- 0.076	32.4 +/- 8.2	37.8
[10] Ct-MGAM N20 & Maltose	2.01 +/- 0.18	27.4 +/- 7.6	13.6
[8] Nt-MGAM & Maltose	4.59 +/- 0.29	9.5 +/- 1.8	2.1

† Number of trials in each average is indicated in superscript

‡ Error is reported as a standard error of the mean

Kinetic parameters for hydrolysis of PNP-glucose are reported Table 5.

Table 5. Kinetic parameters for α-glucosidases with PNP-glucose substrate

†Enzyme-Substrate Pair	K_m (mM) ‡	k_{cat} (s^{-1}) ‡	k_{cat}/K_m ($s^{-1}mM^{-1}$)
[4] Nt-SI & PNP-Glucose	2.32 +/- 0.055	2.3 +/- 0.2	1.01
[5] Ct-SI & PNP-Glucose	8.18 +/- 0.76	0.4 +/- 0.08	0.05
[3] Ct-MGAM N2 & PNP-Glucose	2.35 +/- 0.80	0.3 +/- 0.1	0.13
[4] Ct-MGAM N20 & PNP-Glucose	3.48 +/- 0.34	0.1 +/- 0.01	0.03
[3] Nt-MGAM & PNP-Glucose	16.7 +/- 2.4	1.9 +/- 0.3	0.11

† Number of trials in each average is indicated in superscript

‡ Error is reported as a standard error of the mean

3.1.2 Inhibition constants associated with maltose and PNP-glucose hydrolysis by mammalian α-glucosidases in the presence of LAB-1 and DAB-1.

Table 6 contains results for inhibition assays involving LAB-1, the separate substrates maltose and PNP-glucose, and all five catalytic subunits. Both mixed and competitive modes of inhibition were observed in the presence of LAB-1. The mode of inhibition associated with each substrate depended on the catalytic subunit under observation. Presence or absence of mixed inhibition, and the extent thereof, also appeared to be influenced by the substrate used.

Table 6. Inhibition constants for LAB-1 with mammalian α-glucosidases

Enzyme-Substrate Pair	K_i (nM)	α	β	Mode of Inhibition
Nt-SI & PNP-Glucose	56.6 +/- 8.7	10.70 +/- 4.76	-	Mixed
Nt-SI & Maltose	29.8 +/- 2.5	6.05 +/- 1.30	-	Mixed
Ct-SI & PNP-Glucose	565 +/- 30	-	-	Competitive
Ct-SI & Maltose	608 +/- 51	10.96 +/- 2.60	-	Mixed
Nt-MGAM & PNP-Glucose	560 +/- 55	7.96 +/- 3.49	-	Mixed
Nt-MGAM & Maltose	413 +/- 33	-	-	Competitive
Ct-MGAM N2 & PNP-Glucose	312 +/- 32	3.42 +/- 0.488	-	Mixed
Ct-MGAM N2 & Maltose	411 +/- 63	4.39 +/- 0.987	-	Mixed
Ct-MGAM N20 & PNP-Glucose	573 +/- 46	-	-	Competitive
Ct-MGAM N20 & Maltose	463 +/- 40	4.46 +/- 0.625	-	Mixed

† Error in each parameter is reported as a standard error of the mean

Likewise, results for assays involving DAB-1 are reported in Table 8. Once again both mixed and competitive inhibition kinetics are observed for different enzyme-substrate pairs in the presence of this inhibitor. Inhibition constants are consistently larger in magnitude for DAB-1 than for LAB-1, indicating that all five subunits have a generally weaker affinity for the D-enantiomer.

Table 7. Inhibition constants for DAB-1 with mammalian α-glucosidases

Enzyme-Substrate Pair	K_i (μM)	α	β	Mode of Inhibition
Nt-SI & PNP-Glucose	1.18 +/- 0.113	13.25 +/- 3.57	-	Mixed
Nt-SI & Maltose	0.500 +/- 0.039	9.47 +/- 2.54	-	Mixed
Ct-SI & PNP-Glucose	5.16 +/- 0.409	-	-	Competitive
Ct-SI & Maltose	4.95 +/- 0.266	-	-	Competitive
Nt-MGAM & PNP-Glucose	3.43 +/- 0.120	-	-	Competitive
Nt-MGAM & Maltose	1.82 +/- 0.171	8.75 +/- 2.06	-	Mixed
Ct-MGAM N2 & PNP-Glucose	2.717 +/- 0.183	8.43 +/- 1.11	-	Mixed
Ct-MGAM N2 & Maltose	2.64 +/- 0.353	6.53 +/- 1.44	-	Mixed
Ct-MGAM N20 & PNP-Glucose	4.82 +/- 0.032	8.55 +/- 0.693	-	Mixed
Ct-MGAM N20 & Maltose	2.80 +/- 0.223	14.11 +/- 2.78	-	Mixed

† Error in each parameter is reported as a standard error of the mean

Results from inhibition assays with palatinose as substrate are excluded here due to the occurrence of substrate inhibition. LAB-1 and DAB-1 were both found to inhibit palatinose hydrolysis by Nt-SI and Nt-MGAM, but mechanistic deductions were not made due to overlap between the range of substrate concentrations used in the inhibition assays, and the range of substrate concentrations that elicited the phenomenon of substrate inhibition.

3.2 Substrate inhibition of palatinose hydrolysis by Nt-SI and Nt-MGAM

Substrate inhibition occurs at elevated substrate concentrations when increasing the concentration of substrate in solution leads to a reduced rate of reaction. At the molecular level, it is generally caused by the formation of enzyme-substrate-substrate (ESS) complexes with reduced or abolished catalytic activity (Purich, 1983). There are several mechanisms by which substrate inhibition can occur: it can be caused by the presence of a second binding site of lower substrate affinity; it may also commonly result from a second substrate molecule binding to a subsite in an already partially occupied binding pocket (Purich, 1983). In the second scenario, two substrate molecules can bind simultaneously in sub-optimal configurations. Resultant ESS complexes may be entirely nonproductive, or they may retain some catalytic activity.

Nt-SI's capacity to hydrolyze palatinose was tested using a broad range of substrate concentrations. The palatinose hydrolysis activity assay was performed as described previously. Subtracting the blank rate observed from the control with no enzyme present was very important, especially at higher substrate concentrations. The blank rate was thought to be caused by contaminating glucose in the substrate. Although the substrate was greater than 99% pure, at very high concentrations, contaminants could be present in significant quantities. The blank rate, determined to be linear with respect to the concentration of palatinose in solution, was subtracted from rates obtained from the assay in question in order to isolate the changes in reaction rate that were solely due to the substrate inhibition phenomenon.

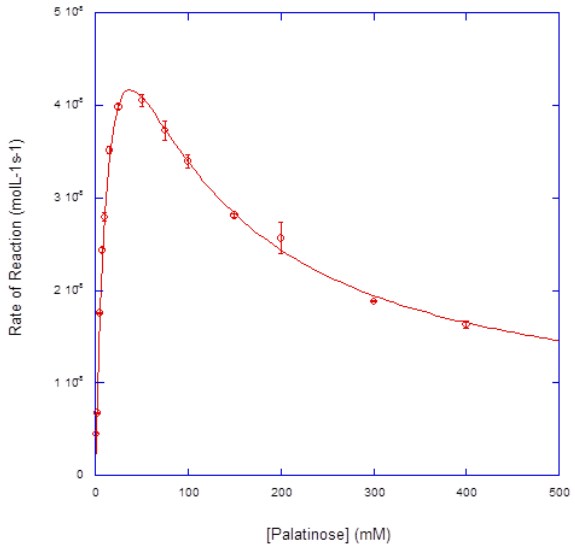

Figure 10. Partial substrate inhibition model for Nt-SI hydrolysis of palatinose. Error bars represent the standard error of the mean.

Results of this assay indicate that at a concentration of approximately 50 mM palatinose, substrate inhibitory effects begin to take place. Data were first fit to a partial substrate inhibition model by nonlinear regression with Kaleidagraph™ software. For this model, the coefficient of determination was 0.998. The rate equation, originally derived by J. B. S. Haldane in 1930 (Haldane, 1930), was obtained from Herbert J. Fromm's publication *Initial Rate Enzyme Kinetics*:

$$v = \frac{V_1 . [1 + \frac{V_2 \cdot [S]}{V_1 \cdot K_i}]}{1 + \frac{K_m}{[S]} + \frac{[S]}{K_i}}$$

Equation 18. Partial substrate inhibition rate equation (Fromm, 1975).

A model for complete substrate inhibition was also considered. The rate equation for this model is

$$v = \frac{V_1 \cdot [S]}{K_m + [S] + \frac{[S]^2}{K_i}}$$

Equation 19. Complete substrate inhibition rate equation (Fromm, 1975).

The complete substrate inhibition model was also an excellent fit, with a coefficient of determination of 0.997.

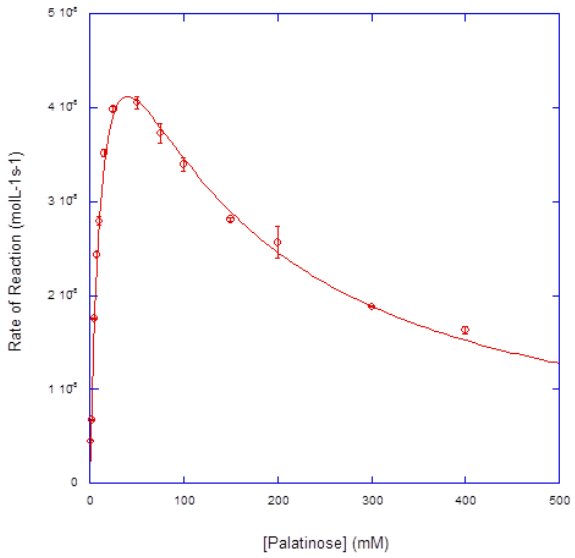

Figure 11. Complete substrate inhibition model for Nt-SI hydrolysis of palatinose.

Since the partial substrate inhibition model does not provide a significantly better fit to the data, it is more likely that the substrate inhibition seen here is complete. Based on structural evidence for multiple subsites within the Nt-SI active site (Sim *et al.*, 2010), the possibility that multiple palatinose molecules are able to bind the enzyme should be considered. Because there is no evidence for presence of a second, lower-affinity binding site for palatinose or other

disaccharide substrates, the concomitant binding of two palatinose molecules to the active site is the preferred hypothesis.

Assuming that the substrate inhibition is complete, the Michaelis constant for the ES (Nt-SI-palatinose) complex is 14.28 mM, while the dissociation constant for the ESS complex is 110.58 mM. A complete substrate inhibition model assumes that as the substrate concentration becomes infinitely high, the rate of reaction will approach zero.

The substrate inhibition seen here is possibly related to the fact that the natural substrate of Nt-SI is isomaltose, a disaccharide composed of glucose subunits which is, like palatinose, linked by an α-1,6 glycosidic bond; of the other catalytic subunits, isomaltase activities have only been observed for Nt-MGAM, and to a much lesser extent (Lee *et al.*, 2014). Palatinose concentrations that elicit this kinetic behaviour are higher than one would generally expect to find in the small intestine under physiological conditions. For this reason, it is quite possible that this substrate inhibition is a phenomenon without great biological significance. It may simply be a product of *in vitro* experimental conditions which do not properly reflect the conditions these enzymes would normally encounter in the mammalian small intestine.

Neither partial nor complete substrate inhibition was observed for any C-terminal catalytic subunits and substrates studied here. Some evidence for substrate inhibition has been observed for Nt-MGAM, although the phenomenon remains to be fully characterized. Preliminary data were modeled using the complete substrate inhibition equation (Equation 13). Based on this model, the Michaelis constant for Nt-MGAM hydrolysis of palatinose is estimated to be 110.89 mM, and the dissociation constant for the ESS complex is estimated to be 278.68 mM.

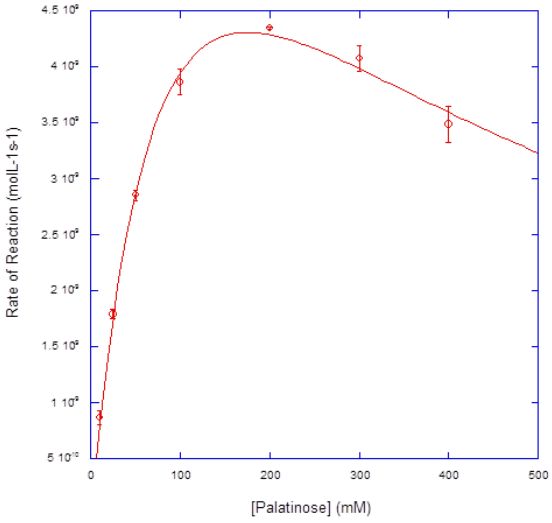

Figure 12. Complete substrate inhibition model for Nt-MGAM hydrolysis of palatinose.

One possible explanation for substrate inhibition in this case is that both the -1 and +1 subsites are occupied respectively by glucose or fructose moieties of two palatinose molecules. For Nt-SI, substrate inhibitory effects appear to begin taking place at much lower concentrations of palatinose than they do for Nt-MGAM, mirroring the difference in Michaelis constants observed for the two enzymes with this substrate.

Table 8. Kinetic parameters for Nt-SI and Nt-MGAM with palatinose substrate

Enzyme-Substrate Pair	K_m (mM)	V_{max} ($molL^{-1}s^{-1}$)	K_i (mM)
Nt-SI & PNP-Glucose	14.28 +/- 1.27	$7.1x10^{-8}$ +/- $3.4x10^{-9}$	110.58 +/- 9.94
Nt-MGAM & PNP-Glucose	110.89 +/- 20.6	$9.7x10^{-9}$ +/- 1.2 $x10^{-9}$	278.68 +/- 63.6

3.3 Inhibition of Nt-SI activities by LAB-1

3.3.1 Inhibition of Nt-SI maltose hydrolysis by LAB-1

Concerning the hydrolysis of maltose, LAB-1 and DAB-1 both inhibit Nt-SI more effectively than they inhibit any of the other catalytic subunits. The K_i value associated with inhibition by LAB-1, 29.8 +/- 2.5 nM, indicates the most potent inhibition observed in any experiments reported here. A physical interpretation of this number is that the inhibitor is able to interact with Nt-SI in a manner that influences the enzyme's ability to bind the substrate maltose. Presumably, when LAB-1 binds to Nt-SI, an EI complex forms, decreasing the amount of free enzyme present. Based on this event, a shift in the chemical equilibrium causes ES complexes present in the reaction mixture to more readily dissociate back to free enzyme and free substrate. The apparent or observed Michaelis constant is increased in the presence of this inhibitor, as a result. A substantial increase in K_m^{app}, dependent on inhibitor concentration, was seen in the presence of LAB-1. The Michaelis-Menten plot for this inhibition assay is illustrated in Figure 13.

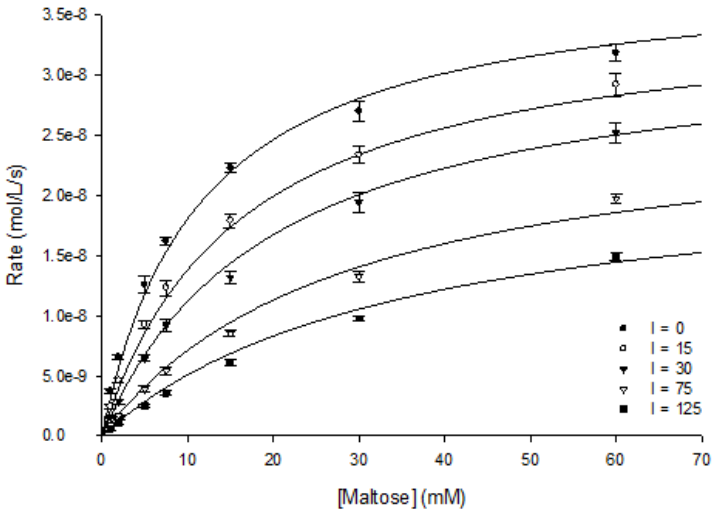

Figure 13. Michaelis-Menten plot for Nt-SI hydrolysis of maltose in the presence of LAB-1.

These data indicated that the inhibitor concentration affected not only on the apparent Michaelis constants, but also the apparent maximal reaction velocity. The apparent V_{max} was decreased in the presence of LAB-1, indicating that this inhibitor and the maltose substrate could be bound to Nt-SI simultaneously. SigmaPlot's Enzyme Kinetics module was used for a global assessment of the family of curves. A full mixed inhibition model for data collected at variable LAB-1 concentrations provided the best fit, ranked first among all kinetic models under consideration, with a coefficient of determination of 0.987. Full and partial models for competitive, mixed, and noncompetitive inhibition were all analyzed; uncompetitive models were excluded on the basis of a very unambiguous increase in magnitude of the parameter K_m in the presence of LAB-1. Full competitive and noncompetitive models yielded respective coefficients of determination of 0.925 and 0.969. Based on these findings, it appears that either this inhibitor can bind the ES complex, or the substrate can bind the EI complex, or both, causing the formation of a non-productive EIS complex.

The following double-reciprocal Lineweaver-Burk plot was also constructed. Lines of the Lineweaver-Burk plot provided a fair fit for the data. Lines were found to intersect very close to but slightly to the left of the ordinate axis. Noticeably higher error was observed for data points which were calculated from the lowest absorbance readings, due to poor spectrophotometer sensitivity at low concentrations of the chromophoric product.

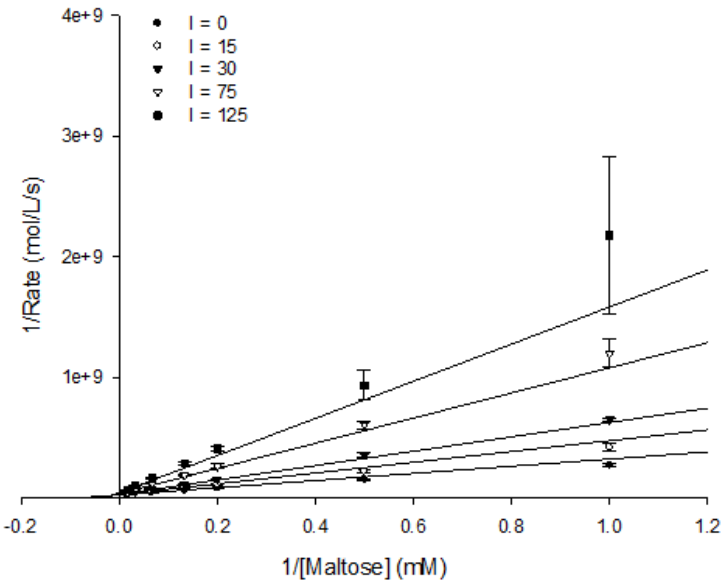

Figure 14. Lineweaver-Burk plot for Nt-SI hydrolysis of maltose in the presence of LAB-1.

The possibility of formation of a productive EIS complex, indicating partial inhibition, was explored via transformation of the data for use in a Dixon plot. This plot illustrates changes in the reciprocal rate of reaction over a range of inhibitor concentrations. When a compound causes complete inhibition, it is expected that the change in the reciprocal rate is linear with respect to a change in the inhibitor concentration. A hyperbolic Dixon plot indicates that at higher inhibitor concentrations, an increase in the inhibitor concentration has much smaller effects on the rate than it does at lower inhibitor concentrations. This can be explained by the formation of a productive EIS complex.

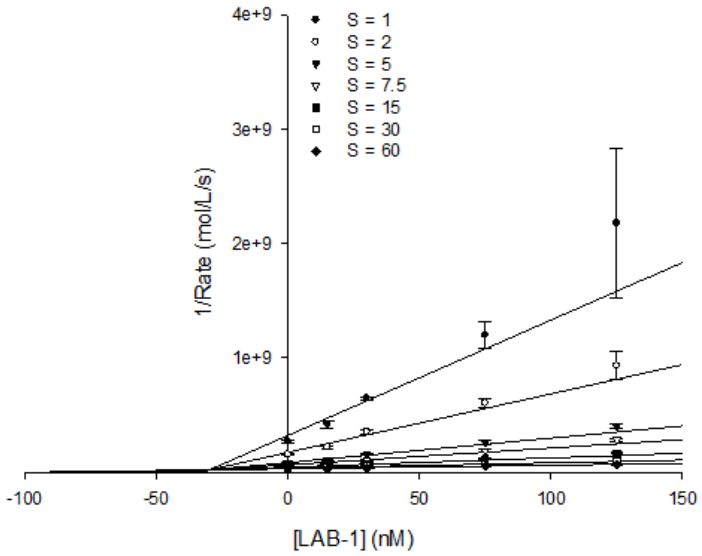

Figure 15. Dixon plot for Nt-SI hydrolysis of maltose in the presence of LAB-1.

Linearity of Dixon plot data points for each substrate concentration indicate that inhibition by LAB-1 is complete rather than partial. Lines appear to intersect at a point with an abscissa of approximately -30 nM. This indicates a K_i value of this magnitude.

Catalytic effects of LAB-1 binding are possibly due to a number of interactions with Nt-SI residues proximal to the -1 subsite. Considering the crystal structure of Nt-SI complexed with kotalanol, it is apparent that acid/base catalyst Asp 571 and catalytic nucleophile Asp 472 (Sim *et al*., 2010) may both be interacting with LAB-1, if its binding configuration is at all similar to that of the five-member ring of kotalanol. LAB-1 may be only partially obstructing the -1 subsite, allowing maltose to still bind, while its hydrogen bonding interaction with Asp 571 and/or Asp 472 may prevent effective catalysis. Asp 355 may also interact with LAB-1 if it binds in the -1 subsite. To implicate a complete and accurate set of residues involved in binding LAB-1, a crystal structure of Nt-SI in complex with this inhibitor is needed.

3.3.2 Inhibition of Nt-SI PNP-glucose hydrolysis by LAB-1

The assay conducted to assess the extent of Nt-SI hydrolysis of PNP-glucose in the presence of LAB-1 yielded data which were, like those obtained from the experiment with maltose, best explained by a mixed-type inhibition model. The global analysis performed using SigmaPlot's Enzyme Kinetics module indicated that a partial mixed model was the best fit, with a coefficient of determination of 0.968. The full mixed model had a coefficient of determination of 0.965. Due to the small difference in goodness of fit of the two models, linearity of the Dixon plot was assessed qualitatively as well. The greater value of R^2 observed for the partial mixed model might simply have been caused by the addition of a redundant parameter (Motulsky, 2014). Evidence for hyperbolic character of lines in the Dixon plot would support the case for a partial mixed model. Dixon plots were therefore carefully considered.

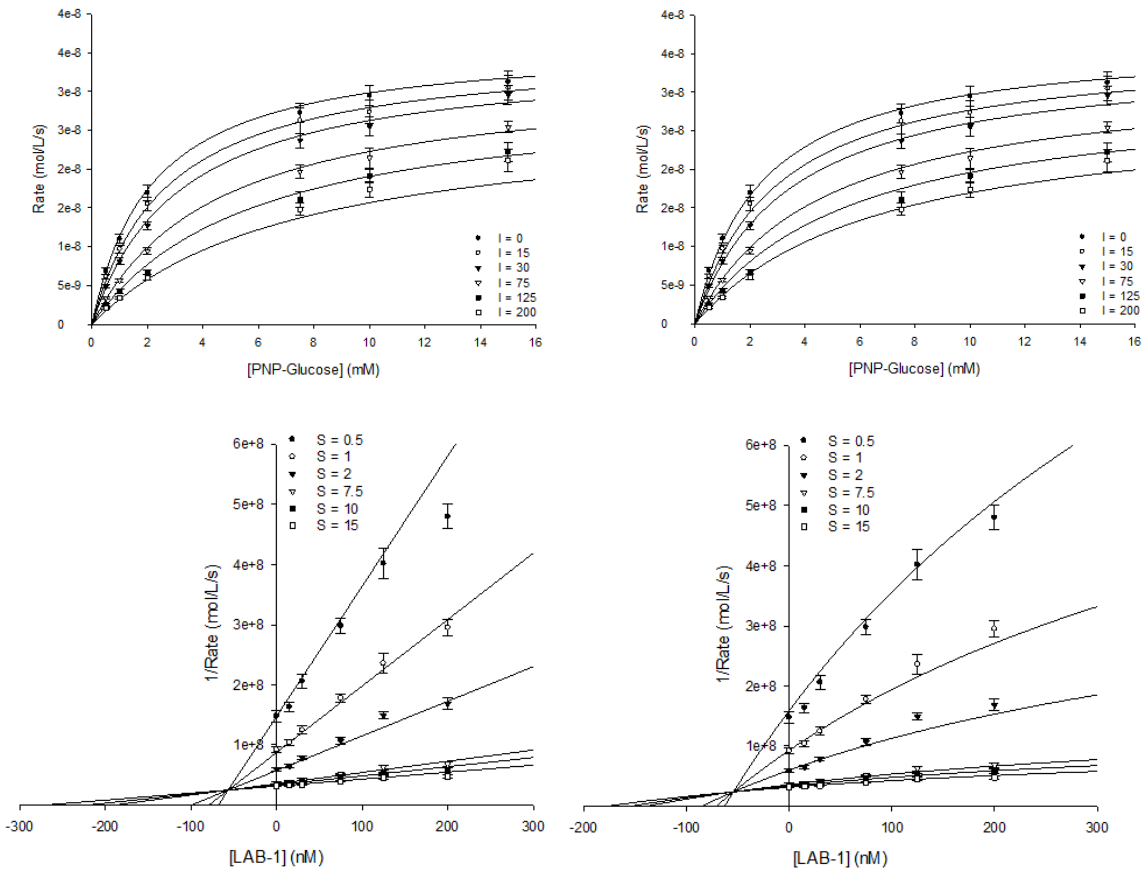

Figure 16. Michaelis-Menten and Dixon plots for Nt-SI hydrolysis of PNP-glucose in the presence of LAB-1; a) Michaelis-Menten plot for full mixed model, b) Michaelis-Menten plot for partial mixed model, c) Dixon plot for full mixed model, d) Dixon plot for partial mixed model.

Both full and partial mixed model Dixon plots appear to fit data points fairly well. Data points from the assay trial at 200 nM LAB-1 appear in some cases to have lower reciprocal rates than the full mixed model would predict. The partial mixed model provides a better fit for the 0.5 mM PNP-glucose point at 200 nM LAB-1. However, this model also provides a poorer fit for other data points, and altogether, these qualitative observations of the Dixon plots do not justify an increase in model complexity. It is possible that the apparent hyperbolic character is

an artifact of the assay procedure, especially since it mainly appears to be due to 200 nM LAB-1 data points alone.

Table 9. Kinetic parameters for partial and full mixed models of LAB-1 inhibition of PNP-glucose hydrolysis by Nt-SI.

Model	K_m (mM)	K_i (nM)	α	β	R^2
Partial Mixed	2.4 +/- 0.2	54.3 +/- 11.8	5.2 +/- 2.0	0.44 +/- 0.14	0.968
Full Mixed	2.2 +/- 0.2	56.6 +/- 8.7	10.7 +/- 4.8	-	0.965

Error in all columns is reported as a standard error of the mean

Assuming a full mixed inhibition model, the K_i is 56.6+/- 8.7 nM, and the value of the parameter α is 10.7. Invoking the principle of parsimony, and due to its general goodness of fit, this remains the preferred model. Furthermore, a replot of K_m^{app}/V_{max}^{app} as a function of LAB-1 concentration was an excellent fit to a linear model, providing no compelling evidence for a partial inhibition.

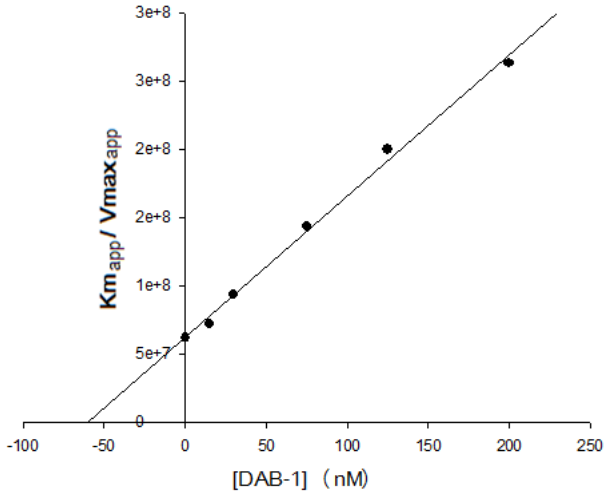

Figure 17. Replot of K_m^{app} / V_{max}^{app} as a function of [LAB-1] for LAB-1 inhibition of PNP-glucose hydrolysis by Nt-SI.

3.4 Inhibition of Ct-SI activities LAB-1

3.4.1 Inhibition of Ct-SI maltose hydrolysis by LAB-1

Inhibition of Ct-SI maltose hydrolysis by LAB-1 was best suited to a full mixed inhibition model. The inhibition constant was found to be 0.608 +/- 0.051 µM, and the parameter α was 10.96 +/- 2.60. A full mixed inhibition model would suggest that LAB-1 is able to bind to both the free enzyme and to the ES complex, exerting effects on the apparent affinity Ct-SI has for maltose, as well as on Ct-SI's catalytic capacity.

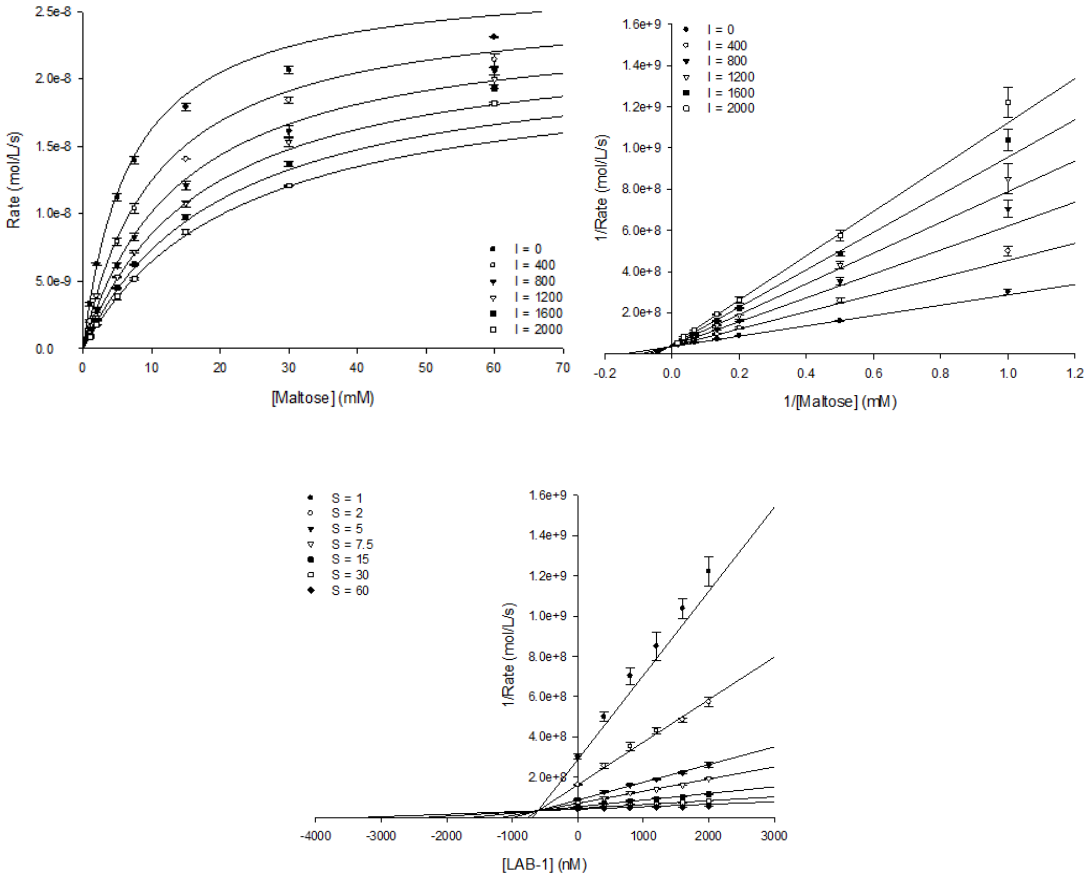

Figure 18. Michaelis-Menten, Lineweaver-Burk, and Dixon plots for Ct-SI hydrolysis of maltose in the presence of LAB-1, assuming a full mixed inhibition model; a) Michaelis-Menten plot, b) Lineweaver-Burk plot, c) Dixon plot.

60 mM maltose data points do not conform as well to this model as the lower substrate concentration data points. This is obvious when one observes both Michaelis-Menten and Dixon plots. The coefficient of determination for the full mixed inhibition model was 0.982. While once again a partial mixed model was ranked highest by R^2, a distinct lack of evidence for hyperbolic character in the Dixon plot indicates that a full inhibition model provides the most suitable explanation for these data.

In a local analysis, estimation of kinetic parameters for individual curves by nonlinear regression does not show a significant change in V_{max} in the presence of LAB-1, and the Lineweaver-Burk plot produced from these data indicates competitive inhibition. That results obtained by the global analysis should contrast those obtained by the individual curve analysis seems counterintuitive. The standard error of the mean for each data point clearly does not account for the apparent displacement of points at 60 mM maltose, so it is unlikely that this is simply an inflated experimental error. Conclusions from the global analysis will be reported here, but reasonable uncertainty in the mode of inhibition should be duly noted.

3.4.2 Inhibition of Ct-SI PNP-glucose hydrolysis by LAB-1

LAB-1 was found to competitively inhibit PNP-glucose hydrolysis by Ct-SI. The full competitive model was ranked highest by R^2, with a value of 0.989. The inhibition constant determined from these data was 0.565 +/- 0.030 µM. This value was very similar to that obtained from the assay with Ct-SI, LAB-1, and maltose, at 0.608 +/- 0.051 µM.

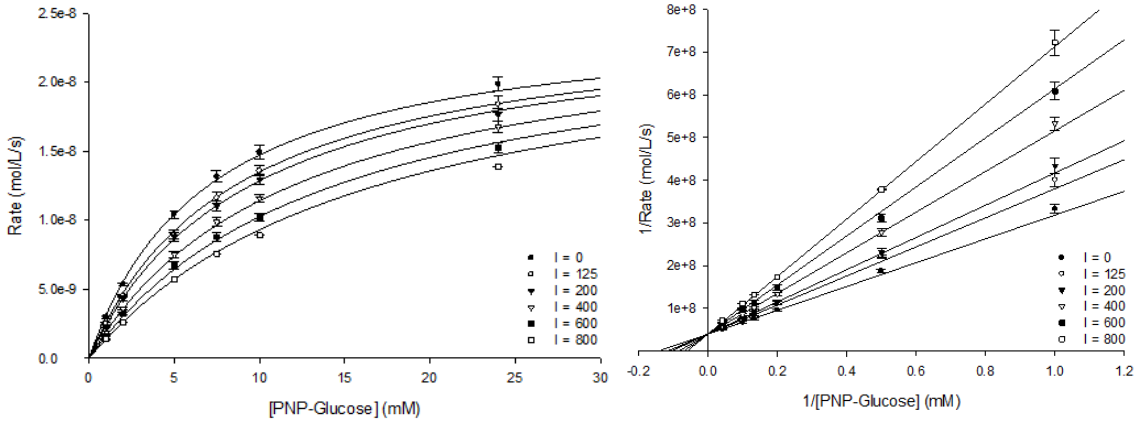

Figure 19. Michaelis-Menten and Lineweaver-Burk plots for Ct-SI hydrolysis of PNP-glucose in the presence of LAB-1, assuming a full competitive inhibition model; a) Michaelis-Menten plot, and b) Lineweaver-Burk plot.

The difference in modes of inhibition between Nt-SI (mixed) and Ct-SI (competitive) in the presence of PNP-glucose implies that, while Nt-SI can apparently accommodate LAB-1 and PNP-glucose binding simultaneously, Ct-SI cannot. Without structural information about the Ct-SI active site, it is difficult to detail the molecular interactions that may lead to this result. It is possible, however, that the shape of the Nt-SI +1 subsite, which is known to be narrower and more spatially constraining than the Nt-MGAM subsite (Sim *et al.*, 2010), is instrumental in determining whether PNP-glucose and LAB-1 can bind simultaneously.

3.5 Inhibition of Nt-MGAM activities LAB-1

3.5.1 Inhibition of Nt-MGAM maltose hydrolysis by LAB-1

LAB-1 was found to inhibit Nt-MGAM maltose hydrolysis competitively ($R^2 = 0.979$), with a K_i value of 0.413 +/- 0.033 µM. Please see Figure 20 for Michaelis-Menten and Lineweaver-Burk plots.

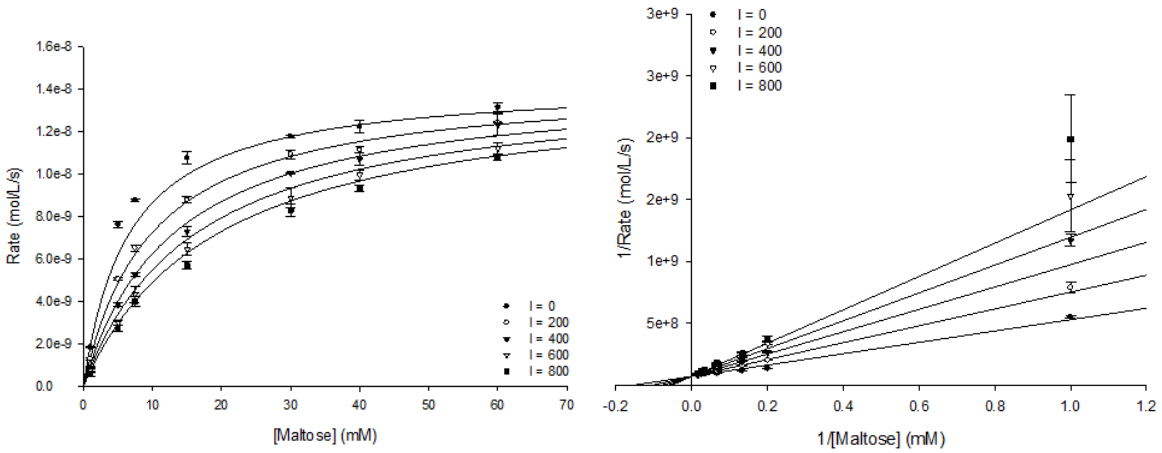

Figure 20. Michaelis-Menten and Lineweaver-Burk plots for Nt-MGAM hydrolysis of maltose in the presence of LAB-1 with full competitive inhibition model; a) Michaelis-Menten plot and b) Lineweaver-Burk plot.

Of the other catalytic subunits, Nt-SI has the highest overall amino acid sequence similarity to Nt-MGAM (Sim *et al.*, 2010), and the -1 subsites of the two enzymes' active sites share many structural features essential to the hydrolysis of substrates such as maltose and PNP-glucose (Sim *et al.*, 2010). Mixed inhibition kinetics observed for Nt-SI and LAB-1 indicate that LAB-1 binds both to Nt-SI and to the Nt-SI-maltose complex, with a marked preference for the free enzyme. Nt-MGAM, however, does not seem to tolerate the simultaneous binding of both maltose and LAB-1. It is logical that if LAB-1 binds in a manner similar to the five-member

ring of kotalanol near the -1 subsite, structural differences in this immediate region should be able to contribute to a hypothesis that would explain the kinetic disparities.

The most pronounced difference in the -1 subsites of these two enzymes is that Nt-SI's Tryptophan 327 is analogous to Tyrosine 299 in Nt-MGAM (Sim *et al*., 2010). Trp 327 in Nt-SI is thought to confer α-1,6 specificity (Sim *et al*., 2010). This residue may be integral to the determination of whether one or both ligands can bind the -1 subsite at once. Differences in the +1 subsite may also be important; constraints placed on the substrate from the narrowness of the Nt-SI +1 subsite, compared with the Nt-MGAM +1 subsite (Sim *et al*., 2010), might actually be necessary for it to bind in the presence of LAB-1.

3.5.2 Inhibition of Nt-MGAM PNP-glucose hydrolysis by LAB-1

A number of models provided excellent fits to data from the LAB-1 inhibition assay with Nt-MGAM and PNP-glucose. A partial mixed inhibition model was considered to be the best fit ($R^2 = 0.992$) and a full mixed model appeared to fairly explain the data as well ($R^2 = 0.979$). Dixon plots were used to compare the full and partial models qualitatively.

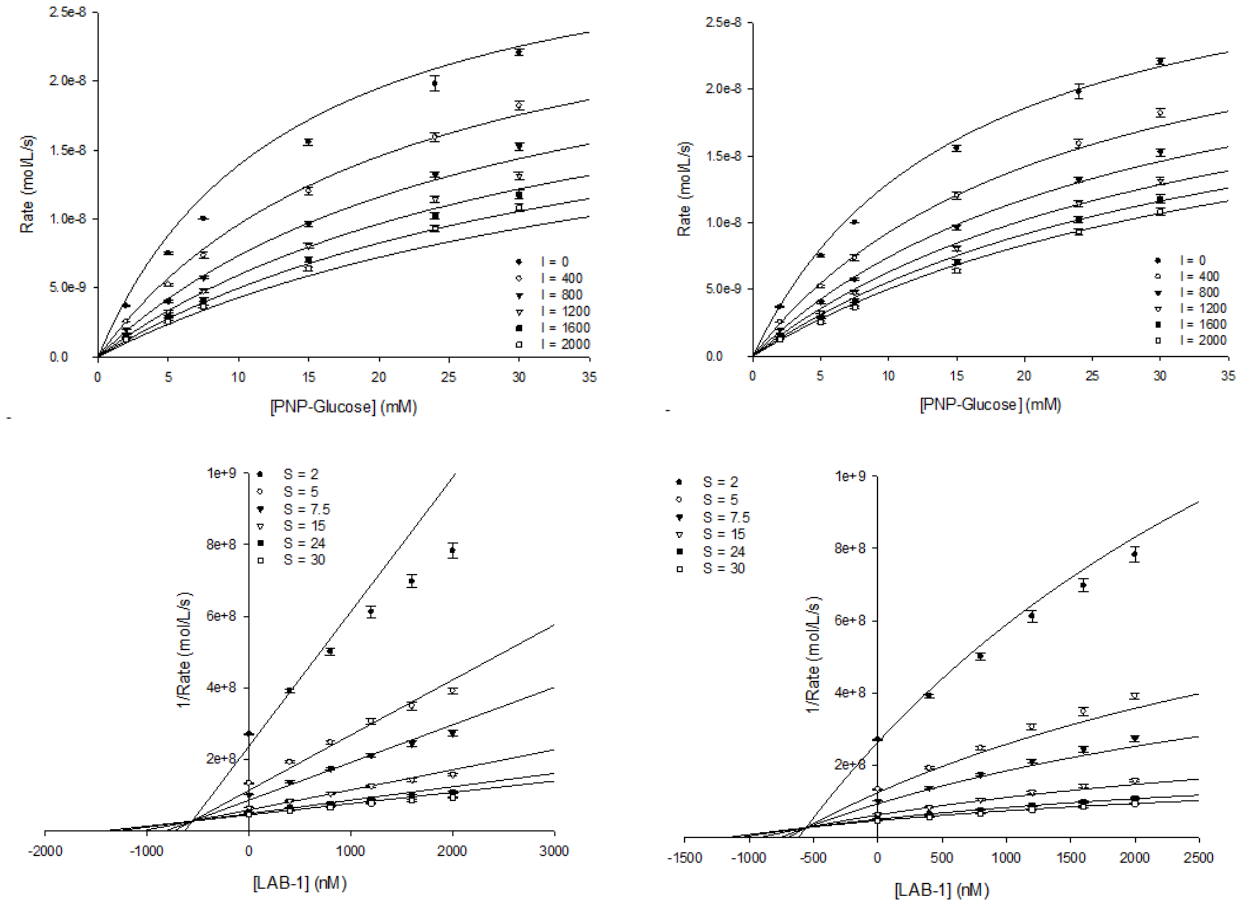

Figure 21. Michaelis-Menten and Dixon plots for Nt-MGAM hydrolysis of PNP-glucose in the presence of LAB-1; a) Michaelis-Menten plot for full mixed model, b) Michaelis-Menten plot for partial mixed model, c) Dixon plot for full mixed model, d) Dixon plot for partial mixed model.

In addition to both mixed models, competitive and noncompetitive models were also assessed. The partial competitive model provided a very poor fit for 2 mM PNP-glucose data points on the Dixon plot, and the full competitive model had a lower coefficient of determination than both mixed models. Noncompetitive models were globally poor fits.

Table 10. Kinetic parameters for partial and full mixed models of LAB-1 inhibition of PNP-glucose hydrolysis by Nt-MGAM.

Model	K_m (mM)	K_i (µM)	α	β	R^2
Partial Mixed	15.2 +/- 0.8	0.560 +/- 0.055	4.49 +/- 0.95	0.43 +/- 0.072	0.992
Full Mixed	13.5 +/- 1.0	0.560 +/- 0.048	7.96 +/- 3.49	-	0.979

Error in all columns is reported as a standard error of the mean

Assuming a full mixed model, K_i was found to be 0.560 +/- 0.055 µM, with an α value of 7.96 +/- 3.49. For the partial mixed model, the inhibition constant was 0.560 +/- 0.048 µM. Parameters α and β were 4.49 +/- 0.95 and 0.43 +/- 0.072, respectively. To further investigate the possibility of hyperbolic inhibition, a secondary replot was constructed, considering K_m^{app} / V_{max}^{app} as a function of [LAB-1].

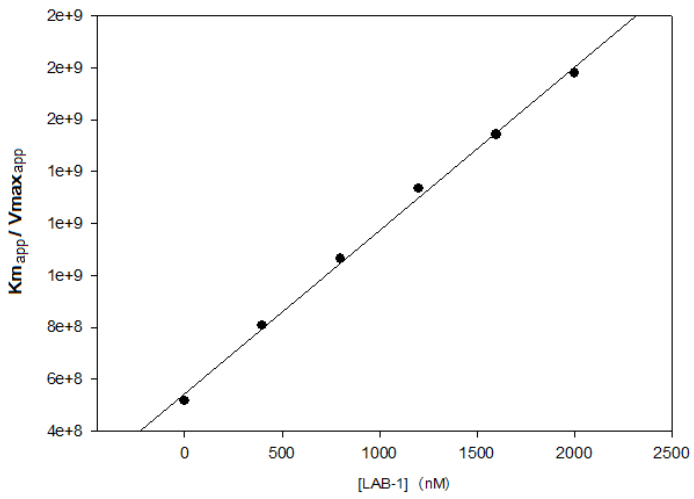

Figure 22. Replot of K_m^{app} / V_{max}^{app} as a function of [LAB-1] for LAB-1 inhibition of PNP-glucose hydrolysis by Nt-MGAM.

The plot of K_m^{app} / V_{max}^{app} as a function of [LAB-1] was well explained by a linear model, with a coefficient of determination of 0.997. Because the pattern of data points had no distinct hyperbolic character, introduction of a partiality factor into the rate equation was considered

unwarranted. The full mixed model, albeit quantitatively a slightly poorer fit to the data, was therefore the preferred model.

PNP-glucose solubility imposed an unfortunate limitation on this particular assay, resulting in sub-optimal representation of Michaelis-Menten curves. With more accurate V_{max} estimates, one would have more confidence that the full mixed model described here reflects the nature of the inhibition taking place.

3.6 Inhibition of Ct-MGAM N2 and N20 activities by LAB-1

3.6.1 Inhibition of Ct-MGAM N2 and N20 maltose hydrolysis by LAB-1

The most suitable model for LAB-1 inhibition of Ct-MGAM N2 maltose hydrolysis was a full mixed model with a K_i value of 0.411 +/- 0.063 μM and an α value of 4.39 +/- 0.99. Michaelis-Menten and Lineweaver-Burk plots are depicted in Figure 23. The full mixed model had a coefficient of determination of 0.945.

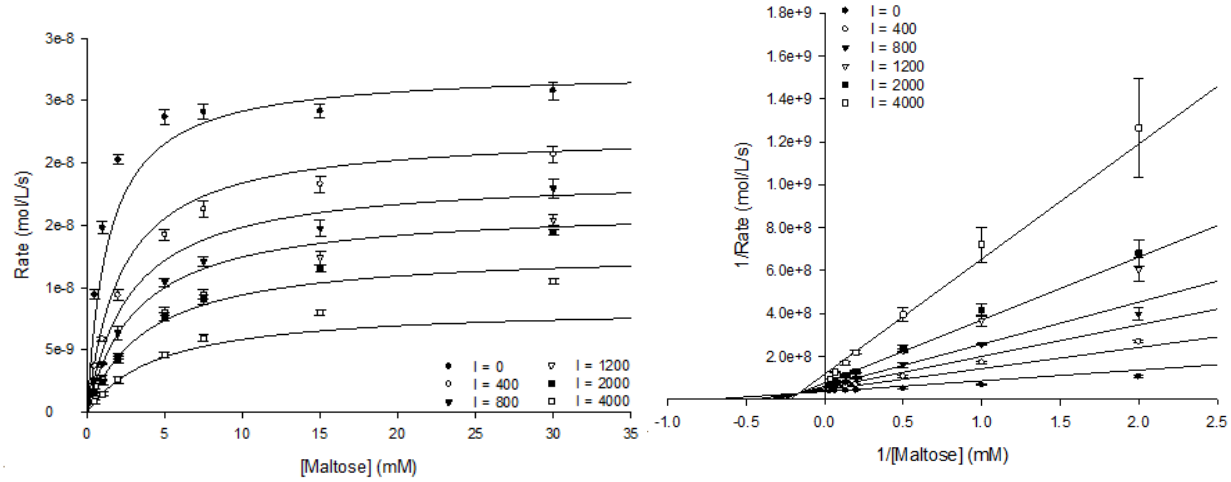

Figure 23. Michaelis-Menten and Lineweaver-Burk plots for Ct-MGAM N2 hydrolysis of maltose in the presence of LAB-1, assuming a full mixed inhibition model.

A partial mixed model was ranked first by R^2 with a value of 0.947, but the Dixon plot for these data did not appear to conform well to the model. The partial mixed model could not properly account for data points at 4000 nM [LAB-1]. Analysis of the Lineweaver-Burk plot for the partial mixed model also indicated a markedly poorer fit to most data points. For these reasons, an additional increase in the complexity of the model was not justified. All other models under consideration were poorer fits to the data, with R^2 values of 0.91 or less.

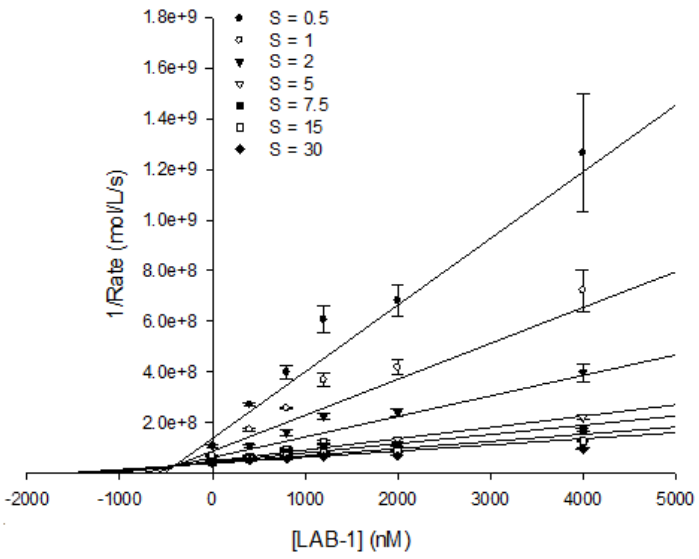

Figure 24. Dixon plot for Ct-MGAM N2 hydrolysis of maltose in the presence of LAB-1, assuming a full mixed inhibition model.

LAB-1 inhibition of Ct-MGAM N20 maltose hydrolysis was also most suited to a full mixed model (R^2 = 0.98) with an inhibition constant of 0.463 +/- 0.040 μM and an α value of 4.46 +/- 0.62. There was no significant difference between inhibition constants and α values obtained from experiments with the two Ct-MGAM isoforms, indicating that they are not differentially inhibited by LAB-1.

The fact that there is no significant difference in the extent or mode of inhibition between the two C-terminal MGAM subunits suggests that the 89-amino acid substitution of Ct-MGAM N20 does not affect binding of LAB-1. The -1 subsite of Ct-MGAM N2 has a number of proximal aspartic acid residues, including Asp 1420, Asp 1526 (potentially an acid/base catalyst), Asp 1279, and Asp 1157. There are many opportunities for hydrogen-bonding with LAB-1 hydroxyl groups in this subsite. Given the potential that Asp 1526 functions as an acid/base catalyst (Ren *et al*., 2011), the obstruction of catalysis might be explained by a contact between the inhibitor LAB-1 and this specific residue. It is interesting, too, that this mode of inhibition is observed for nt-SI and both Ct-MGAM isoforms in the presence of maltose, while it is not observed for Nt-MGAM.

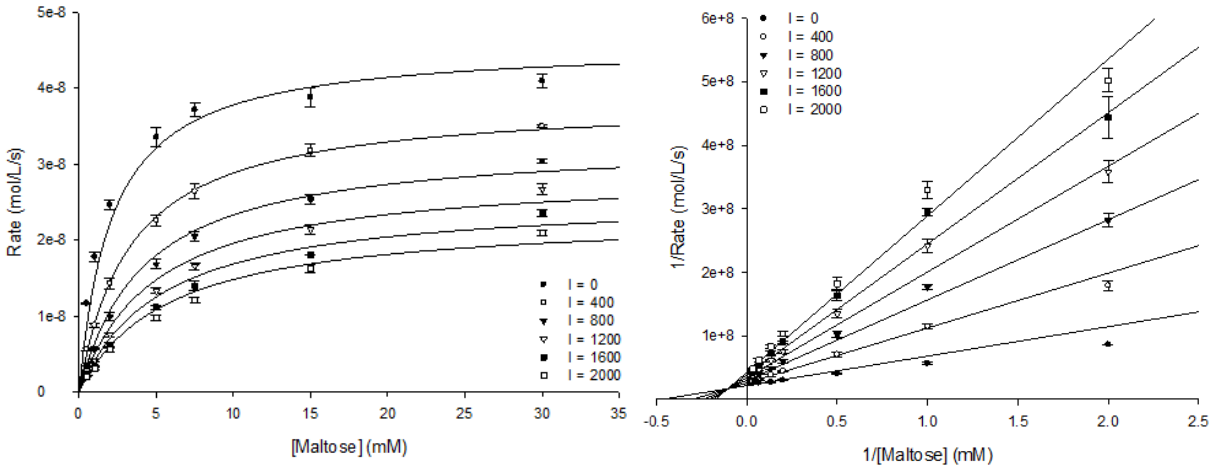

Figure 25. Michaelis-Menten and Lineweaver-Burk plots for Ct-MGAM N20 hydrolysis of maltose in the presence of LAB-1, assuming a full mixed inhibition model.

3.6.2 Inhibition of Ct-MGAM N2 and N20 PNP-glucose hydrolysis by LAB-1

Data for LAB-1 inhibition of Ct-MGAM N2 PNP-glucose hydrolysis was best fit by a full mixed model, which yielded a K_i value of 0.312 +/- 0.032 µM and an α value of 4.39 +/- 0.99 (R^2 = 0.98). These values are highly similar to mixed inhibition parameters determined for Ct-MGAM N2 and N20 hydrolysis of maltose in the presence of LAB-1. This supports the conclusion that the two isoforms are affected to the same extent and most likely in the same way by the binding of LAB-1.

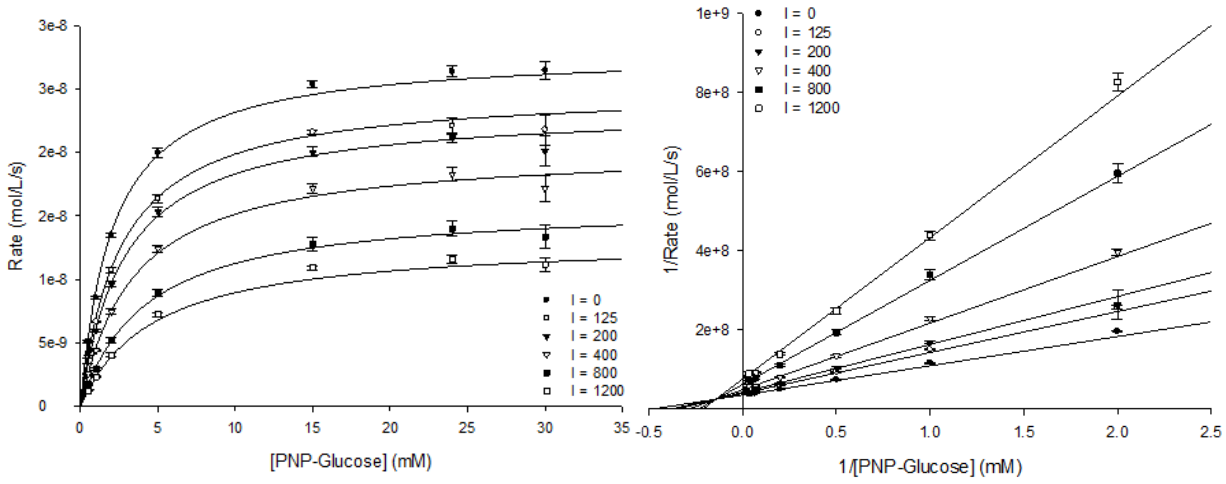

Figure 26. Michaelis-Menten and Lineweaver-Burk plots for Ct-MGAM N2 hydrolysis of PNP-glucose in the presence of LAB-1, assuming a full mixed inhibition model.

LAB-1 inhibition of Ct-MGAM N20 PNP-glucose hydrolysis was best described by a full competitive inhibition model with a K_i value of 0.573 +/- 0.046 µM. The model had a coefficient of determination of 0.985. A partial mixed model was found to have higher R^2 value (0.989), but the difference was not considered substantial enough to warrant introduction of an additional parameter. The Dixon plot did not have any appreciable hyperbolic character.

The full competitive model fit high substrate concentration data points quite poorly, and for this reason, the possibility of mixed inhibition in this case was also explored. An alternative analysis was performed whereby estimation of local kinetic parameters for individual curves was done by nonlinear regression. The Lineweaver-Burk plot from this analysis also indicated competitive inhibition, as lines were found to intersect at the ordinate axis. Based on a qualitative judgment, it is likely that the error associated with 25 mM substrate data points is due to experimental error. The confidence associated with this conclusion is therefore rather low.

3.7 Inhibition of Nt-SI activities by DAB-1

3.7.1 Inhibition of Nt-SI maltose hydrolysis by DAB-1

DAB-1 inhibition of Nt-SI maltose hydrolysis conformed well to a full mixed inhibition model ($R^2 = 0.98$). The inhibition constant was found to be 0.500 +/- 0.039 μM, and the α value was 9.47 +/- 2.54. If a mixed model does fairly characterize these inhibition kinetics, then it should be concluded that LAB-1 and DAB-1 both reduce Nt-SI's affinity for maltose and interfere with the mechanism of catalysis. The K_i value associated with inhibition by LAB-1 is ~17 times smaller in magnitude than the K_i value associated with inhibition by DAB-1, and catalytic effects caused by LAB-1 are also evidently more substantial.

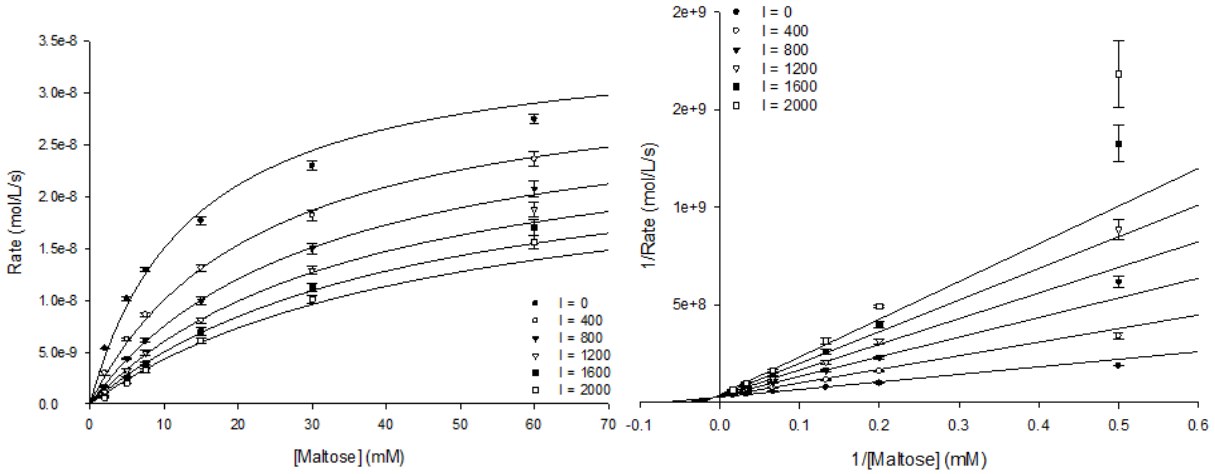

Figure 27. Michaelis-Menten and Lineweaver-Burk plots for Nt-SI hydrolysis of maltose in the presence of DAB-1, assuming a full mixed inhibition model.

The Dixon plot for these data revealed that 2 mM maltose data points conform rather poorly to the full mixed model. Once again, increased error at low substrate concentrations is most likely the result of spectrophotometer error from low absorbance values. Unsurprisingly, the error observed here is more pronounced at higher DAB-1 concentrations. The Dixon plot provides good evidence for a full, rather than partial, inhibition model.

3.7.2 Inhibition of Nt-SI PNP-glucose hydrolysis by DAB-1

As was observed with the substrate maltose, DAB-1 inhibition of Nt-SI PNP-glucose hydrolysis is best described by a full mixed inhibition model ($R^2 = 0.981$). A partial mixed model was ranked first by R^2 ($R^2 = 0.986$), but there is not sufficient curvature in the Dixon plot to warrant an increase in model complexity. Reciprocal rates associated with 4000 nM DAB-1 data points on the Dixon plot are indeed generally lower than the full mixed model would predict, but this pattern does not appear to hold for data points associated with lower DAB-1

concentrations. The full mixed model provided an inhibition constant of 1.18 +/- 0.113 µM and an α value of 13.25 +/- 3.57.

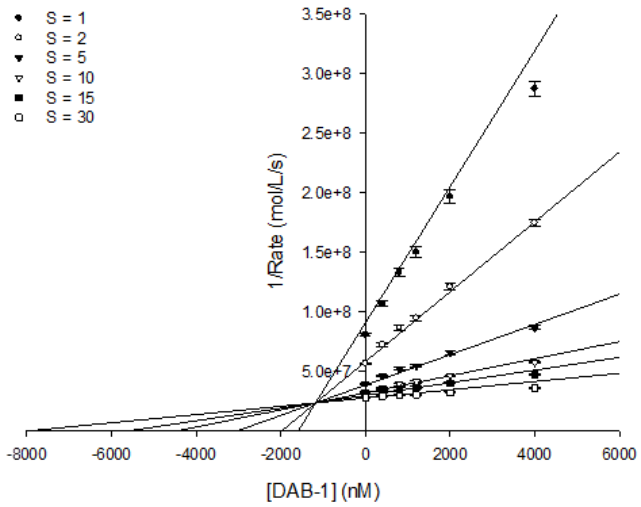

Figure 28. Dixon plot for Nt-SI hydrolysis of PNP-glucose in the presence of DAB-1, assuming a full mixed inhibition model.

3.8 Inhibition of Ct-SI activities by DAB-1

3.8.1 Inhibition of Ct-SI maltose hydrolysis by DAB-1

The K_i value for DAB-1 inhibition of Ct-SI maltose hydrolysis was determined to be 4.95 +/- 0.266, assuming a full competitive inhibition model (R^2 = 0.988). These inhibition kinetics are distinct from kinetics of LAB-1 inhibition, which were best suited to a full mixed model. The LAB-1 inhibition constant was ~8 times smaller in magnitude than that of DAB-1.

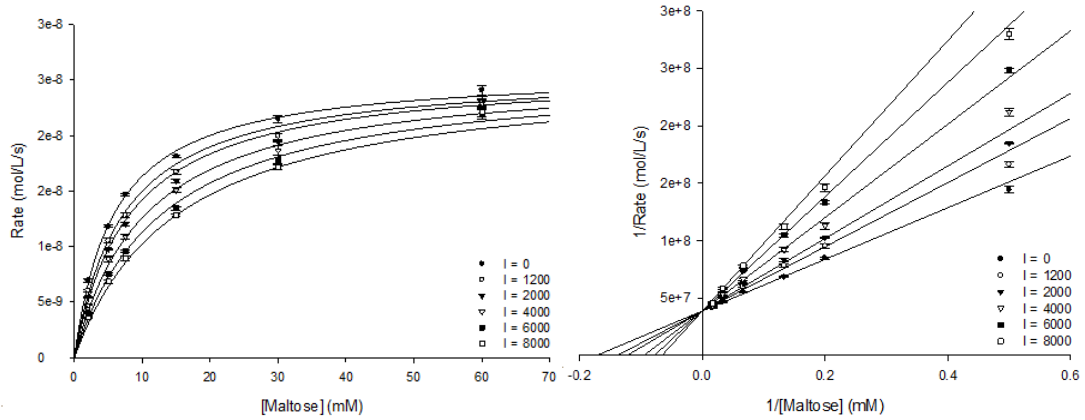

Figure 29. Michaelis-Menten and Lineweaver-Burk plots for Ct-SI hydrolysis of maltose in the presence of DAB-1, assuming a full competitive inhibition model.

3.8.2 Inhibition of Ct-SI PNP-glucose hydrolysis by DAB-1

The best model for DAB-1 inhibition of PNP-glucose hydrolysis by Ct-SI was a partial mixed model (R^2 = 0.986), with an inhibition constant of 2.37 +/- 0.302 µM. Parameters α and β were determined to be 2.69 +/- 0.38 and 0.60 +/- 0.043, respectively. This mode of inhibition is quite different from the full competitive model which best characterizes DAB-1 inhibition of maltose hydrolysis by Ct-SI. A full competitive model was applied to these data as well, but the coefficient of determination was only 0.974. Parameters associated with both full competitive and partial mixed models are reported below in Table 11.

Table 11. Kinetic parameters for partial mixed and full competitive models of DAB-1 inhibition of PNP-glucose hydrolysis by Ct-SI.

Model	K_m (mM)	K_i (µM)	α	β	R^2
Partial Mixed	5.4 +/- 0.3	2.37 +/- 0.30	2.69 +/- 0.38	0.60 +/-0.043	0.986
Full Competitive	5.7 +/- 0.3	5.16 +/- 0.41	-	-	0.974

Error in all columns is reported as a standard error of the mean

Michaelis-Menten plots are depicted in Figure 30.

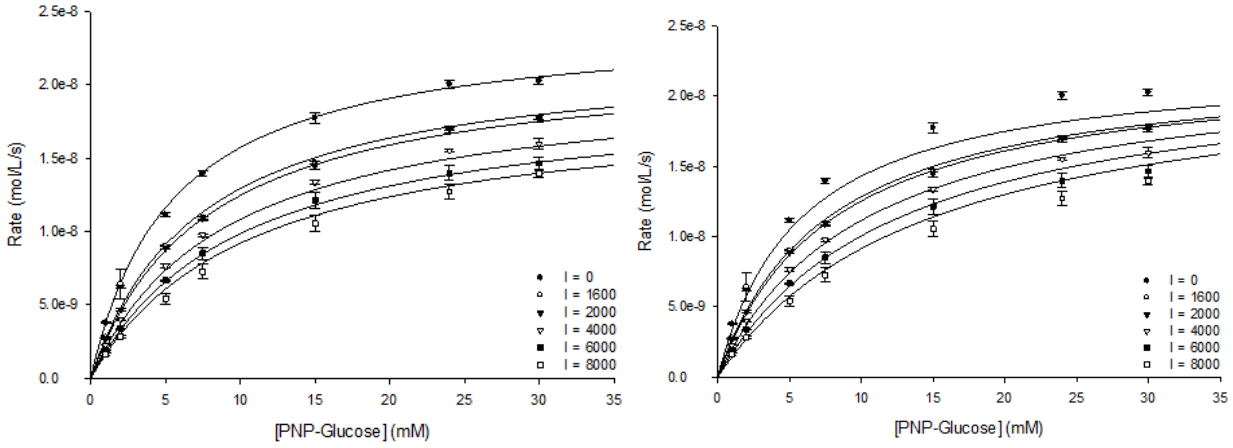

Figure 30. Michaelis-Menten plots for Ct-SI hydrolysis of PNP-glucose in the presence of DAB-1; a) partial mixed model, and b) full competitive model.

Dixon plots for partial and full mixed inhibition models were also compared. Points on the Dixon plot are fit better by the partial mixed model, but the difference in goodness of fit may simply be due to generally higher error associated with points obtained at low substrate and high inhibitor concentrations, due to spectrophotometer limitations discussed previously.

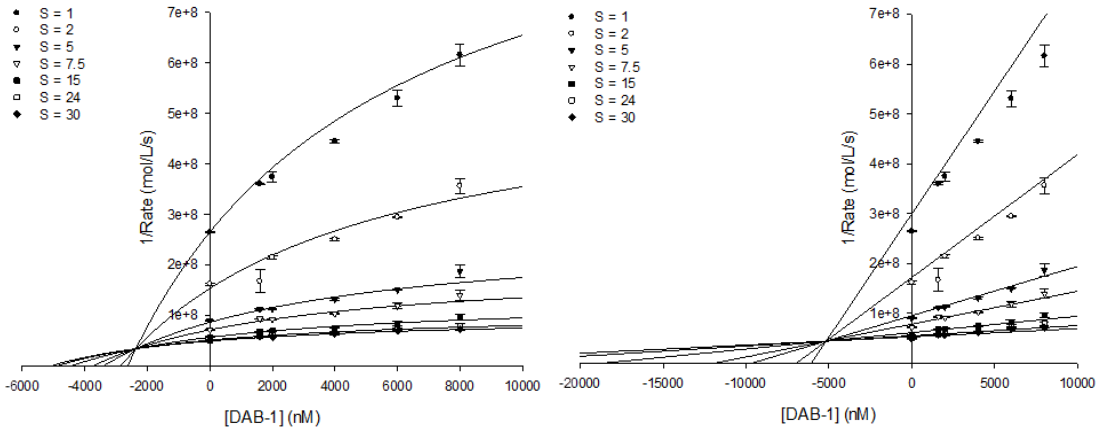

Figure 31. Dixon plots for Ct-SI hydrolysis of PNP-glucose in the presence of DAB-1; a) partial mixed model, and b) full competitive model.

A secondary plot of K_m^{app}/V_{max}^{app} was constructed to assist in the determination of whether introduction of a partiality factor into the inhibition model was justified. Points on this

plot were explained well by a linear model (R^2 = 0.964), indicating a lack of evidence for hyperbolic inhibition. The full competitive model was therefore considered the most appropriate model to explain the data.

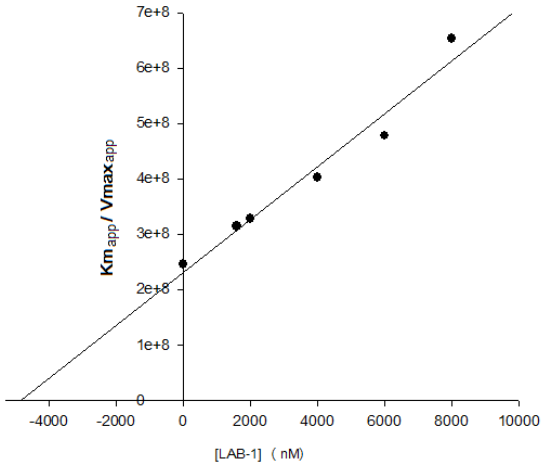

Figure 32. Replot of K_m^{app} / V_{max}^{app} as a function of [DAB-1] for DAB-1 inhibition of PNP-glucose hydrolysis by Ct-SI.

3.9 Inhibition of Nt-MGAM activities by DAB-1

3.9.1 Inhibition of Nt-MGAM maltose hydrolysis by DAB-1

Assuming a full mixed inhibition model (R^2 = 0.976), the K_i value for DAB-1 inhibition of Nt-MGAM was determined to be 1.82 +/- 0.171 μM. The α value was 8.75 +/- 2.06. A full competitive model was a much poorer fit to the data (R^2 = 0.943). Mixed inhibition by DAB-1 would contrast the competitive inhibition of this subunit that was seen with LAB-1.

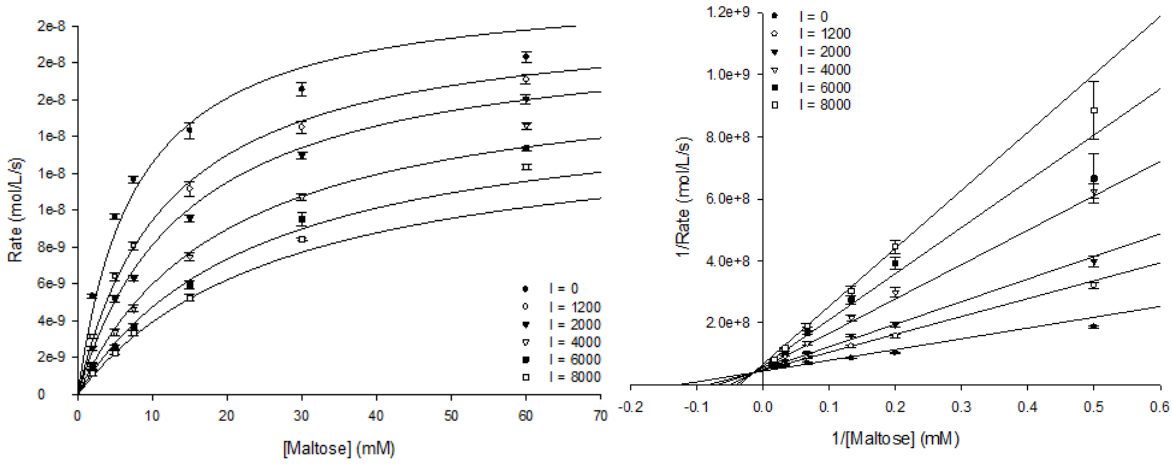

Figure 33. Michaelis-Menten and Lineweaver-Burk plots for Nt-MGAM hydrolysis of maltose in the presence of DAB-1, assuming a full mixed inhibition model.

The Michaelis-Menten plot depicted in Figure 33 recalls the same poor fit for 60 mM maltose data points that was seen in the assay with Ct-SI, where a full mixed model was also selected as the best model for these data by the global analysis. The conclusion regarding whether the inhibition is truly mixed or competitive should therefore be regarded with some uncertainty.

3.9.2 Inhibition of Nt-MGAM PNP-glucose hydrolysis by DAB-1

PNP-glucose hydrolysis by Nt-MGAM was competitively inhibited by DAB-1, with an inhibition constant of 3.43 +/- 0.120 µM. The full competitive inhibition model had a coefficient of determination of 0.993, ranking below both partial mixed and partial competitive models. The disparity in R^2 values for the three models was very small, and the Dixon plot does not overwhelmingly favour a partial inhibition model. For these reasons, the full competitive model was deemed best. The Michaelis-Menten and Dixon plots are depicted in Figure 34.

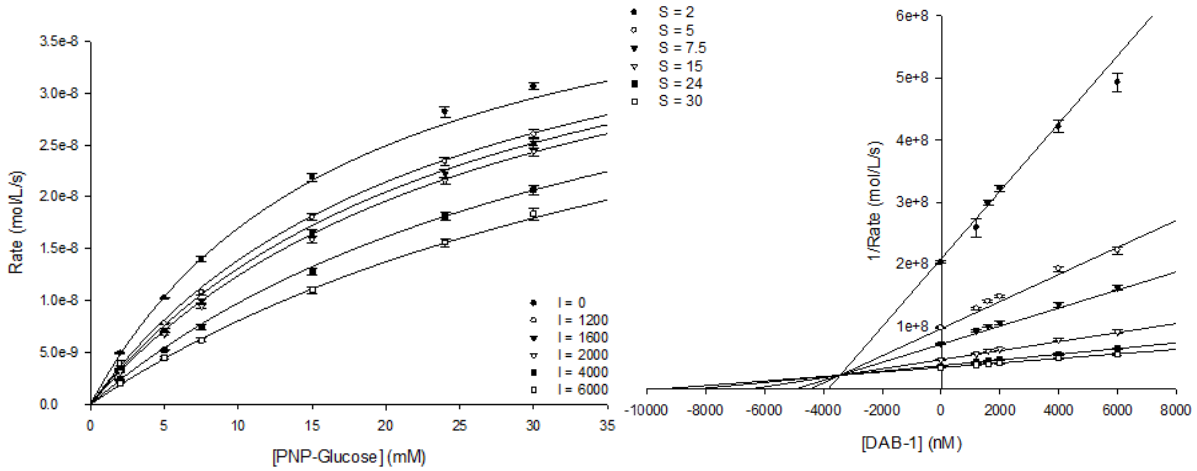

Figure 34. Michaelis-Menten and Dixon plots for Nt-MGAM hydrolysis of PNP-glucose in the presence of DAB-1, assuming a full competitive inhibition model.

.

Once again, PNP-glucose solubility imposed limitations on V_{max} estimates that could be extracted from this dataset. This presents a source of error and limits the amount of mechanistic information that can be extracted from the dataset.

3.10 Inhibition of Ct-MGAM N2 and N20 activities by DAB-1

3.10.1 Inhibition of Ct-MGAM N2 and N20 maltose hydrolysis by DAB-1

Ct-MGAM N2 inhibition by DAB-1 was best described by a full mixed inhibition model (R^2 = 0.959). K_i and α values were 2.64 +/- 0.353 µM and 6.53 +/- 1.44 respectively. Michaelis-Menten and Lineweaver-Burk plots are depicted in Figure 35.

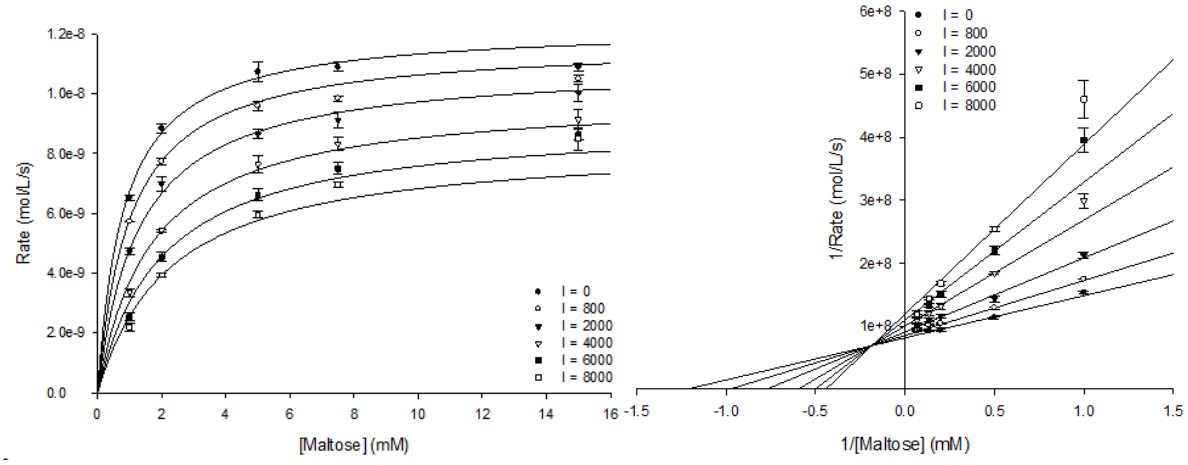

Figure 35. Michaelis-Menten and Lineweaver-Burk plots for Ct-MGAM N2 hydrolysis of maltose in the presence of DAB-1, assuming a full mixed inhibition model.

DAB-1 also exhibited mixed inhibition kinetics with Ct-MGAM N20 and maltose (R^2 = 0.984). The K_i and α values for this inhibition were 2.80 +/- 0.223 µM and 14.22 +/- 2.78. The parameter α assigned to DAB-1 inhibition of Ct-MGAM N20 is more than twice the magnitude of that associated with inhibition of Ct-MGAM N2. Inhibition constants for DAB-1 with both enzymes are almost indiscriminable. Once again it is obvious that the highest substrate concentration data points – in this case, 15 mM maltose – fit the mixed model more poorly than lower substrate concentration data points.

3.10.2 Inhibition of Ct-MGAM N2 and N20 PNP-glucose hydrolysis by DAB-1

Inhibition of Ct-MGAM N2 PNP-glucose hydrolysis by DAB-1 was best fit by a full mixed model, as was the case with maltose as substrate. The coefficient of determination for this model was 0.991. K_i and α values were found to be 2.717 +/- 0.183 µM and 8.43 +/- 1.11 respectively.

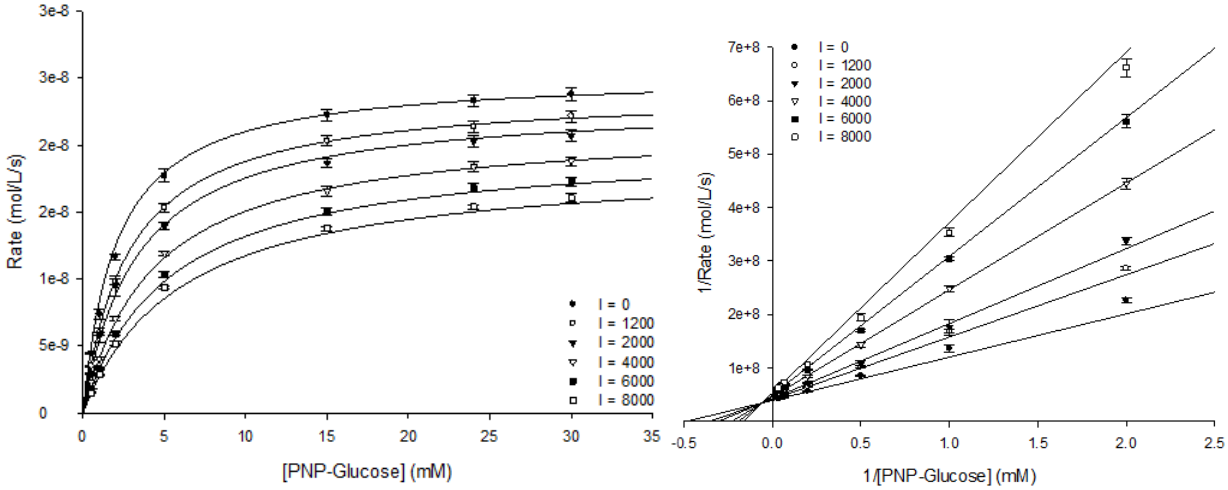

Figure 36. Michaelis-Menten and Lineweaver-Burk plots for Ct-MGAM N2 hydrolysis of PNP-glucose in the presence of DAB-1, assuming a full mixed inhibition model.

A partial mixed inhibition model was ranked first by R^2 (0.993), but the difference between this value and that determined for the full mixed model was minute. This was not considered sufficient evidence of partial inhibition. The Dixon plot is depicted in Figure 37.

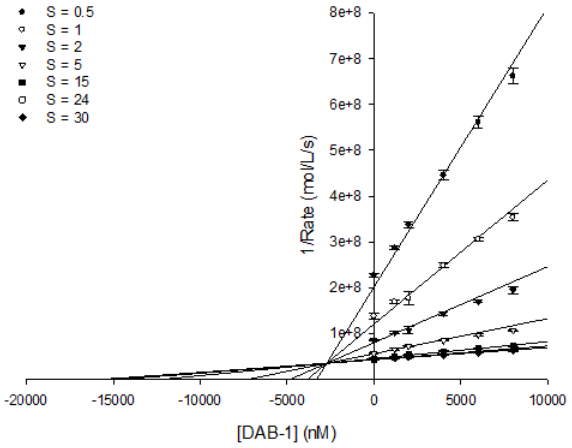

Figure 37. Dixon plot for Ct-MGAM N2 hydrolysis of PNP-glucose in the presence of DAB-1, assuming a full mixed inhibition model.

DAB-1 inhibition of PNP-glucose hydrolysis by Ct-MGAM N20 was found to have a K_i value of 5.22 +/- 0.531, assuming full competitive inhibition. There are a number of problems with this model: firstly, 30 mM PNP-glucose data points are not well accounted for, and secondly, the spread of data points at each substrate concentration is poorly explained. The R^2 value was only 0.961. By observing the Michaelis-Menten plot, one can see that 30 mM PNP-glucose data points are likely higher than they should be, possibly due to experimental error in the execution of the assay. If all 30 mM PNP-glucose data points are associated with erroneously high rates, then the competitive inhibition model is most likely not accurate.

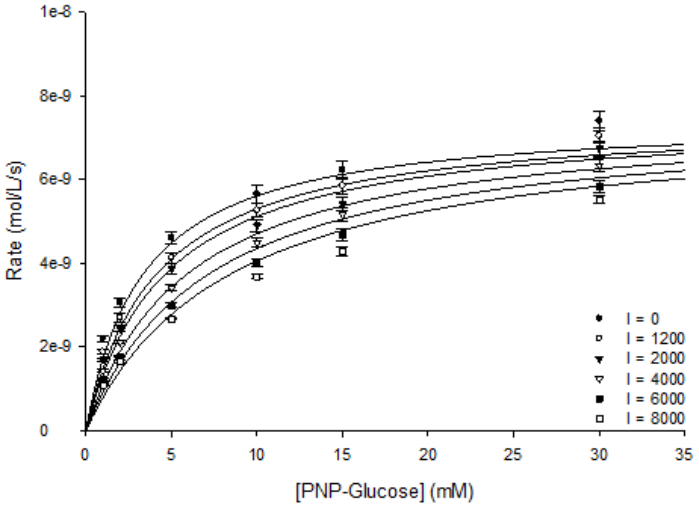

Figure 38. Michaelis-Menten plot for Ct-MGAM N20 hydrolysis of PNP-glucose in the presence of DAB-1, assuming a full competitive inhibition model.

The possibility of mixed inhibition in this case was explored further. Local kinetic parameters for individual curves were estimated by nonlinear regression. The Lineweaver-Burk plot from this analysis indicated mixed inhibition. Calculating inhibition parameters by this method, the K_i was found to be 4.82 +/- 0.0317 µM and the α value was found to be 8.55 +/- 0.693. Because the global and local methods of analysis indicated two different modes of inhibition, the matter was settled qualitatively. The competitive model from the global analysis

was an inexplicably poor fit for 30 mM PNP-glucose data points, while the analysis of individual curves did not predict the same poor fit at only one PNP-glucose concentration value. The mixed model is therefore considered a better qualitative explanation for the data seen here.

Chapter 4 Conclusions

The higher inhibitory potency of LAB-1, compared to DAB-1, has been well-established for rat intestinal α-D-glucosidases in general (Asano *et al*., 2005). This trend was also observed in kinetic data from the present experiments. To attempt to account for the difference, it could be that one or both of the inhibitors may bind at more than one site on the enzymes, or that LAB-1 stereochemistry allows for additional interactions that DAB-1 does not have when it binds. While the former hypothesis is favoured by some (Asano *et al*., 2005), there is as yet no concrete evidence for an alternate binding site for either LAB-1 or DAB-1 on the mammalian α-glucosidases studied here.

Here we have seen that Nt-SI hydrolysis of the disaccharide substrates maltose and PNP-glucose is more powerfully affected by LAB-1 than it is by DAB-1. If the two inhibitors do happen to bind at the same site, then the stereochemistry of pyrrolidine ring hydroxyl groups must somehow contribute to this difference in potency. Observing the Nt-SI crystal structure, solved in complex with the thiosugar sulfonium sulfate inhibitor kotalanol (Sim *et al*., 2010), I hypothesize that LAB-1 and DAB-1 both bind to the -1 subsite of the active site of Nt-SI, where the five-member ring of kotalanol is known to bind. I also hypothesize that this is the general way in which these iminosugars inhibit the activities of all five enzymes studied here.

The -1 subsites of Nt-SI and Nt-MGAM are highly structurally conserved, with very few stark differences (Sim *et al*., 2010). Their +1 subsites exhibit more structural variability, and this is thought to account for the observed differences in substrate specificity (Sim *et al*., 2010). The main -1 subsite difference between the two N-terminal human α-glucosidases is that the

residue Trp 327 in Nt-SI is analogous to Nt-MGAM's Tyr 299. This residue may play a role in favouring LAB-1 binding. A number of aspartic acid residues in the -1 subsite of Nt-SI, including Asp 472, Asp 355, and Asp 571, could form hydrogen bonds with LAB-1 hydroxyl groups. The orientation of hydroxyl groups would largely determine the strength of interactions with these residues in the -1 subsite, and this seems to be the most plausible explanation for the disparity in LAB-1 and DAB-1 potencies. Since it is likely that the heteroatom extension of kotalanol influences the orientation of its five-membered ring in the Nt-SI and Nt-MGAM active sites, the suggestion that DAB-1, with the same ring stereochemistry as kotalanol, binds in precisely the same way, is highly speculative. One molecular docking study has shown that LAB-1 derivatives do very likely bind in the enzyme's active site in the manner discussed here (Kato *et al*., 2015). They showed that hydrogen bonding with inhibitor hydroxyl groups and certain CH-π interactions are essential determinants of the predicted binding capacities of LAB-1 derivatives (Kato *et al*., 2015).

Mixed inhibition of Nt-SI activities by both LAB-1 and DAB-1 could be caused by direct interactions with residues Asp 571, the acid/base catalyst, and Asp 472, the catalytic nucleophile (Sim *et al*., 2010). Since these residues are proximal to the -1 subsite, they could interact directly with any of the hydroxyl groups of LAB-1 and DAB-1. Mixed inhibition kinetics dictate that a substrate and an inhibitor can bind simultaneously to an enzyme, so lacking evidence for an alternate binding site, the preferred hypothesis is that each of the inhibitors is able to bind to Nt-SI in complex with maltose and PNP-glucose substrates. The resultant complex (ESI) is most likely catalytically inactive, based on the preferred full inhibition model. This leads one to believe that one or more catalytic residues is hindered by the binding of these inhibitors. The proposed scheme, wherein LAB-1 and DAB-1 bind to the -1 subsite of the Nt-SI active site,

seems congruent with this finding. If this is the case, LAB-1 and DAB-1 must bind in such a way that they do not completely obstruct binding of the substrate. The fact that thiosugar sulfonium sulfate inhibitors including salacinol and kotalanol have been characterized as competitive inhibitors suggests that the heteroatom extension plays a very important role in blocking the substrate. LAB-1 and DAB-1 lack the heteroatom extension, and they do not exhibit exclusively competitive inhibition kinetics with Nt-SI.

Full mixed inhibition kinetics were observed with most enzyme-substrate pairs tested here, but in some cases, the inhibition was best explained by a full competitive model. Considering the possibility that LAB-1 and DAB-1 bind to the -1 subsite of each enzyme's active site, structural differences in the -1 subsite could contribute to these observations. A few convincing cases of competitive inhibition were observed with Nt-MGAM and with Ct-SI. This mode of inhibition could be related to the shape of the +1 subsites of these enzymes; it has been hypothesized that the narrowness of the Nt-SI +1 subsite is integral to the binding of α-1,6-linked substrates (Sim *et al.*, 2010; Kato *et al.*, 2015). Perhaps Nt-MGAM and Ct-SI +1 subsites do not exercise sufficient constraints on the substrate to allow it to bind simultaneously with LAB-1 or DAB-1.

Ct-MGAM N2 and Ct-MGAM N20 were inhibited by both LAB-1 and DAB-1, and the former inhibitor was found to be more potent than the latter by an order of magnitude. Mixed inhibition was observed with both compounds. The Ct-MGAM isoform N2 structure (Ren *et al.*, 2011) offers some structural insights that may help explain this mode of inhibition. Firstly, if these inhibitors bind to the -1 subsite, there are more aspartic acid residues (five) possibly available for hydrogen bonding contacts in Ct-MGAM N2 than there are in -1 subsites of either

Nt-SI or Nt-MGAM (three). Either the acid/base catalyst or catalytic nucleophile could be hindered directly by the binding of LAB-1 and DAB-1, in this scenario.

Finally, the complete substrate inhibition observed for both Nt-SI and Nt-MGAM at high millimolar concentrations of palatinose may be a phenomenon of biological significance if the result is also applicable to the hydrolysis of isomaltose. Palatinose is only consumed in small quantities – mainly in honey (Oizumi *et al*., 2007) – so the phenomenon seen here does not likely have very much direct significance. It is certainly more likely to be an artifact of the experimental conditions. Still, if the same substrate inhibition is observed for isomaltose, it could indicate that the phenomenon plays a role in moderating glucose release by slowing the hydrolysis of α-1,6-linked starch branch points. A similar phenomenon has been observed with maltase glucoamylase and maltooligosaccharides with up to five units of glucose per substrate molecule (Quezada-Calvillo *et al*., 2007; Quezada-Calvillo *et al*., 2008).

Ultimately, the work reported here confirms that LAB-1 is a more potent inhibitor of all intestinal α-glucosidases tested than is DAB-1. LAB-1 exhibits its most potent inhibitory activity against Nt-SI, and inhibits all other catalytic subunits to a similar extent. Considering the existing Nt-SI, Nt-MGAM, and Ct-MGAM N2 crystal structures, it appears that the mixed inhibition kinetics observed with both inhibitors might be attributable to direct hydrogen bonding interactions with catalytic residues proximal to the -1 subsite in each subunit's active site.

Chapter 5 Future Directions

Numerous inhibitory compounds have already been designed on the basis of LAB-1 and DAB-1 structures (Kato *et al.*, 2015; Carreiro *et al*., 2014). Hydrophobic carbon chains and benzyl groups have been added to the pyrrolidine rings in separate ventures to explore the effects of particular alterations (Kato *et al.*, 2015; Carreiro *et al*., 2014). One possibility that has not been tested, to my knowledge, is the introduction of a sulfur atom as the heteroatom in the pyrrolidine ring of an otherwise LAB-like compound. This could help determine the significance of the type of heteroatom, and in the absence of a crystal structure in complex with this inhibitor, it could perhaps also provide more insights as to how the inhibitor binds.

Since pyrrolidine iminosugars have proven to be effective inhibitors of many different glycoside hydrolases, the question of binding promiscuity *in vivo* remains an important one (Asano *et al*., 2005). Because of the impressive potency of LAB-1 as an α-glucosidase inhibitor, it would be worthwhile to better characterize the interactions that this inhibitor has with different human enzymes. Salacinol and analogues have been shown to inhibit a *Drosophila* homolog of human Golgi α-mannosidase II (Kuntz *et al*., 2005) and whether iminosugar inhibitors LAB-1 and DAB-1 have similar effects remains to be seen.

Crystallization and structure determination for Ct-MGAM N20 and Ct-SI would prove very useful, as well, in developing an understanding of the inhibitory mechanisms and differences in potency associated with LAB-1 and DAB-1. Crystal complexes with human intestinal α-glucosidases and either LAB-1 or DAB-1 could also provide a wealth of information about how and where the inhibitors really bind.

It still seems curious that LAB-1 and DAB-1 can exhibit mixed inhibition, while salacinol and its analogues are exclusively competitive inhibitors (Rossi *et al*., 2006; Sim, 2010; Sim *et al*., 2010; Jones *et al*., 2011). While salacinol and derivatives have DAB-1ike hydroxyl group orientation about the five-member ring, they also each possess a large heteroatom extension. I have put forward the possibility that the heteroatom extension is crucial to the pure competitive nature of the inhibition by salacinol and its derivatives. It would be interesting to see if creating and testing salacinol analogues with heteroatom extensions of varying length might indicate the point at which the inhibitor's heteroatom extension becomes so large that it obstructs binding of the substrate altogether.

Finally, whether or not there is any benefit to purposefully designing mixed inhibitors of mammalian small intestinal α-glucosidases is worthy of some consideration. Most α-glucosidase inhibitors used in the management of type two diabetes are purely competitive. Effectively it seems there is really no benefit to one type of inhibition over the other; the most important goal is to selectively inhibit particular catalytic subunits with different compounds. In any case, it is my hope that the findings reported here will one day be of aid in the development of more highly selective and effective α-glucosidase inhibitors.

References

Andersen, B., Rassov, A., Westergaard, N., and Lundgren, K. **1999**. Inhibition of glycogenolysis in primary rat hepatocytes by 1,4-dideoxy-1,4-imino-arabinatol. *Biochemical Journal*, 342: pp. 545-550.

Asano, N. **2003**. Glycosidase inhibitors: update and perspectives on practical use. *Glycobiology*, 13(10): pp. 93R-104R.

Asano, N., Ikeda, K., Yu, L., Kato, A., Takebayashi, K., Adachi, I., Kato, I., Ouchi, H., Takahata, H., and Fleet, G. W. J. **2005**. The L-enantiomers of D-sugar-mimicking iminosugars are noncompetitive inhibitors of D-glycohydrolase? *Tetrahedron Asymmetry*, 16: pp. 223-229.

Asano, N., Nash, R. J., Molyneux, R. J., and Fleet, G. W. J. **2000**. Sugar-mimic glycosidase inhibitors: natural occurrence, biological activity and prospects for therapeutic application. *Tetrahedron Asymmetry*, 11: pp. 1645-1680.

Auricchio, S., Semenza, G., and Rubino, A. **1965**. Multiplicity of human intestinal disaccharidases: II. Characterization of the individual maltases. *Biochimica et Biophysica Acta*, 96: pp. 498-507.

Butters, T. D., Dwek, R. A., and Platt, F. M. **2005**. Imino sugar inhibitors for treating the lysosomal glycosphingolipidoses. *Glycobiology*, 15(10): pp. 43R-52R.

Butterworth, P. J. **1972**. The use of Dixon plots to study enzyme inhibition. *Biochimica et Biophysica Acta*, 289: pp. 251-253.

Cantarel, B., Coutinho, P., Rancurel, C., Bernard, T., Lombard, V., and Henrissat, B. **2009**. The carbohydrate-active enzymes database (CAZy): an expert resource for glycogenomics. *Nucleic Acids Research*, 37: pp. D233-D238.

Carreiro, E. P., Louro, P., Adriano, Gize, Guedes, A. R., Vannuchi, N., Costa, A. R., Antunes, C. M. M., Guedes, R. C., and Burke, A. J. **2014**. 3-Hydroxypyrrolidine and (3,4)-dihydroxypyrrolidine derivatives: Inhibition of rat intestinal α-glucosidase. *Bioorganic Chemistry*, 54: pp. 81-88.

Cleland, W. W. **1967**. Enzyme kinetics. *Annual Review of Biochemistry*, 36(1): pp. 77-112.

Clugston, M. and Flemming, R. **2000**. Advanced chemistry. Malaysia: *Oxford University Press*. pp. 168.

Copeland, R. A. **2000**. Enzymes: A practical introduction to structure, mechanism, and data analysis. Second Edition. New York: *Wiley-VCH*. pp. 117-122.

Cornish-Bowden, A. **1997**. New beer in an old bottle: Eduard Buchner and the growth of biochemical knowledge. Valéncia; Spain: *Universitat de Valéncia*. pp. 136.

Dahlqvist, A. **1961**. Determination of maltase and isomaltase activities with a glucose-oxidase reagent. *Biochemical Journal*, 80 (3): pp. 547-551.

Davies, G. and Henrissat, B. **1995**. Structures and mechanisms of glycosyl hydrolases. *Structure*, 3(9): pp. 853-859.

de Melo, E. B., da Silveira Gomes, A., and Carvalho, I. **2006**. α- and β-glucosidase inhibitors: Chemical structure and biological activity. *Tetrahedron* 62: pp. 10277-10302.

Evans, S. V., Fellows, L. E., Shing, T. K. M., and Fleet, G. W. J. **1985**. Glycosidase inhibition by plant alkaloids which are structural analogues of monosaccharides. *Phytochemistry*, 24(9): pp. 1953-1955.

Fleet, G. W. J., Karpas, A., Dwel, R., Fellows, L. E., Tyms, A. S., Petursson, S., Namgoong, S. K., Ramsden, N. G., Smith, P. W., Son, J. C., Wilson, F., Witty, D. R., Jacob, G. S., and Rademacher, T. W. **1988**. Inhibition of HIV replication by amino-sugar derivatives. *FEBS Letters* 237(1,2): pp. 128-132.

Fleet, G. W. J., Nicholas, S. J., Smith, P. W., Evans, S. V., Fellows, L. E., and Nash, R. J. **1985**. Potent competitive inhibition of α-galactosidase and α-glucosidase activity by 1,4-dideoxy-1,4-iminopentitols: syntheses of 1,4-dideoxy-1,4-imino-D-lyxitol and of both enantiomers of 1,4-dideoxy-1,4-iminoarabinatol. *Tetrahedron Letters*, 26(26): pp. 3127-3130.

Florez, J. C. **2008**. Newly identified loci highlight beta cell dysfunction as a key cause of type 2 diabetes: Where are the insulin resistance genes? *Diabetologia*, 51: pp. 1100-1110.

Fromm. H. J. **1975**. Initial rate enzyme kinetics. Springer-Verlag, Heidelberg. *Molecular Biology, Biochemistry, and Biophysics*, 22: pp. 144-146.

Furukawa, J., Okuda, S., Saito, K., and Hatanaka, S. **1985**. 3,4-Dihydroxy-2-hydroxymethylpyrrolidine from *Arachniodes standishii*. *Phytochemistry*, 24(3): pp. 593-594.

Gallienne, E., Benazza, M., Gemailly, G., Bolte, J., and Lemaire, M. **2005**. Short synthesis of new salacinol analogues and their evaluation as glycosidase inhibitors. *Tetrahedron*, 61(19): pp. 4557-4568.

Gallienne, E., Gefflaut, T., Bolte, J., and Lemaire, M. **2006**. Synthesis of new nitrogen analogues of salacinol and deoxynojirimycin and their evaluation as glycosidase inhibitors. *Journal of Organic Chemistry*, 71: pp. 894-902.

Gerich, J. E. **2000**. Insulin resistance is not necessarily an essential component of type 2 diabetes. *Journal of Clinical Endocrinology and Metabolism*, 85(6): pp. 2113-2115.

Ghavami, A., Johnston, B. D., Jensen, M. T., Svensson, B., and Pinto, B. M. **2001**. Synthesis of nitrogen analogues of salacinol and their evaluation as glycosidase inhibitors. *Journal of the American Chemical Society*, 123: pp. 6268-6271.

Gray, G., Lally, B., and Conklin, K. **1979**. Action of intestinal sucrase-isomaltase and its free monomers on an α-limit dextrin. *Journal of Biological Chemistry*, 254: pp. 6038-6043.

Greimel, P., Spreitz, J., Stutz, A. E., and Wrodnigg, T. M. **2003**. Iminosugars and relatives as antiviral and potential anti-infective agents. *Current Topics in Medicinal Chemistry*, 3(5): pp. 513-523.

Haldane, J. B. A. **1930**. Enzymes. London: *Longmans*.

Henri, V. **1903**. Lois générales de l'action des diastases. *Librairie Scientifique A. Hermann*.

Horne, G., Wilson, F. X., Tinsley, J., Williams, D. H., and Storer, R. **2011**. Iminosugars pase, present and future: medicines for tomorrow. *Drug Discovery Today*, 16(3,4): pp. 107-118.

Humphries, M. J., Matsumoto, K., White, S. L., and Olden, K. **1986**. Inhibition of experimental metastasis by castanospermine in mice: blockage of two distinct stages of tumor colonization by oligosaccharide processing inhibitors. *Cancer Research*, 46(10): pp. 5215-5222.

Ishida, N., Kumagai, K., Niida, T., Tsuruoka, T., Yumoto, H. **1967**. Nojirimycin, a new antibiotic. II. Isolation, characterization, and biological activity. *Journal of Antibiotics*, 20(2): pp. 66-71.

Jacob, R., Purschel, B., and Naim, H. Y. **2002**. Sucrase is an intramolecular chaperone located at the C-terminal end of the sucrase-isomaltase enzyme complex. *Journal of Biological Chemistry*, 277(35): pp. 32141-32148.

Jayawardena, M. H. S., de Alwis, N. M. W., Hettigoda, V., and Fernando, D. J. S. **2005**. A double blind randomised placebo controlled cross over study of a herbal preparation containing *Salacia reticulata* in the treatment of type 2 diabetes. Journal of *Ethnopharmacology*, 97(2): pp. 215-218.

Jones, K., Sim, L., Mohan, S., Kumarasamy, J., Liu, H., Avery, S., Naim, H. Y., Quezada-Calvillo, R., Nichols, B. L., Pinto, B. M., and Rose, D. R. R. **2011**. Mapping the intestinal alpha-glucogenic enzyme specificities of starch digesting maltase-glucoamylase and sucrase-isomaltase. *Bioorganic & Medicinal Chemistry*, 19: pp. 3929-3934.

Kato, A., Zhang, Z., Wang, H., Jia, Y., Yu, C., Kinami, K., Hirokami, Y., Tsuji, Y., Adachi, I., Nash, R., Fleet, G., Koseki, J., Nakagome, I., and Hirono, S. **2015**. Design and synthesis of labystegines, hybrid iminosugars from LAB and calystegine, as inhibitors of intestinal α-glucosidases: Binding conformation and interaction for Nt-SI. *Journal of Organic Chemistry*, 80: pp. 4501-4515.

Koshland, D. E. Jr. **1953**. Stereochemistry and the mechanism of enzymatic reactions. *Biological Reviews*, 28(4): pp. 416-436.

Krasikov, V. V., Karelov, D. V., and Firsov, L. M. **2001**. α-Glucosidases. *Biochemistry (Moscow)*, 66(3): pp. 267-281.

Krentz, A. J., and Bailey, C. J. **2005**. Oral antidiabetic agents: current role in type 2 diabetes mellitus. *Drugs*, 65(3): pp.385-411.

Kuntz, D., Ghavami, A., Johnston, B. D., Pinto, B. M., and Rose, D. R. **2005**. Crystallographic analysis of the interactions of *Drosophila melanogaster* Golgi α-mannosidase II with the naturally occurring glycomimetic salacinol and its analogues. *Tetrahedron: Asymmetry*, 16: pp. 25-32.

Lajtha, A., Baker, G., Dunn, S., and Holt, A. **2007**. Handbook of neurochemistry and molecular neurobiology: Practical neurochemistry methods, volume 6. Third Ed. New York; New York*: Springer Science & Business Media, LLC*. Chapter 4.

Lee, B., Lin, A., Nichols, B., Jones, K., Rose, D. R., Quezada-Calvillo, R., and Hamaker, B. R. **2014**. Mucusal C-terminal maltase-glucoamylase hydrolyzes large size starch digestion products that may contribute to rapid postprandial glucose generation. *Molecular Nutrition & Food Research*, 58: pp. 1111-1121.

Leskovac, V. **2003**. Comprehensive enzyme kinetics. New York: *Kluwer Academic/Plenum Publishers*. Chapters 5-6.

Lillelund, V. H., Jensen, H. H., Liang, X., and Bols, M. **2002**. Recent developments of transition-state analogue glycosidase inhibitors of non-natural product origin. *Chemical Reviews*, 102(2): pp. 515-553.

Lillioja, S., Mott, D. M., Spraul, M., Ferraro, R., Foley, J. E., Ravussin, E., Knowler, W. C., Bennett, P. H., and Bogardus, C. **1993**. Insulin resistance and insulin secretory

dysfunction as precursors of non-insulin-dependent diabetes mellitus. Prospective studies of Pima Indians. *New England Journal of Medicine*, 329: pp. 1988-1992.

Lombard, V., Golaconda Ramulu, H., Drula, E., Coutinho, P. M., and Henrissat, B. **2014**. The Carbohydrate-active enzymes database (CAZy) in 2013. *Nucleic Acids Research*, 42: pp. D490–D495.

Marles, R. J., and Farnsworth, N. R. **1995**. Antidiabetic plants and their active constituents. *Phytomedicine*, 2(2): pp. 137-189.

McCarter, J. D. and Withers, S. G. **1994**. Mechanisms of enzymatic glycoside hydrolysis. *Current Opinion in Structural Biology*, 4: pp. 885-892.

Meyers, R. A. **1995**. Molecular biology and biotechnology: A comprehensive desk reference. New York: *Wiley-VCH*. pp. 298.

Minami, I., Kuriyama, C., Ikeda, K., Kato, A., Takebayashi, K., Adachi, I., Fleet, G. W., Kettawan, A., Okamoto, T., and Asano, N. **2008**. Effect of five-membered sugar mimics on mammalian glycogen-degrading enzymes and various glucosidases. *Bioorganic & Medicinal Chemistry*, 16(6): pp. 2734-2740.

Mohan, S., and Pinto, B. M. **2007**. Zwitterionic glycosidase inhibitors: salacinol and related analogues. *Carbohydrate Research*, 342: pp. 1551-1580.

Molyneux, R. J., Gardner, D. R., James, L. F., and Colegate, S. M. **2002**. Polyhydroxy alkaloids: chromatographic analysis. *Journal of Chromatography* A., 967(1): pp. 57-74.

Motulsky, H. **2014**. Intuitive Biostatistics. 3rd Ed. New York: *Oxford University Press.* Chapters 35-36.

Muraoka, O., Xie, W., Tanabe, G., Amer, M., Minematsu, T., Yoshikawa, M. **2008**. On the structure of the bioactive constituent from Ayurvedic medicine *Salacia reticulata*: revision of the literature. *Tetrahedron Letters*, 49(51): pp. 7315-7317.

Naim, H., Sterchi, E., and Lentze, M. **1988**. Structure, biosynthesis, and glycosylation of human small intestinal maltase-glucoamylase. *Journal of Biological Chemistry*, 263: pp. 19709-19717.

Nash, R. J., Bell, A., and Williams, J. M. **1985**. 2-hydroxymethyl-3,4-dihydroxypyrrolidine in fruits of *Angylocalyx boutiqueanus*. *Phytochemistry*, 24(7): pp. 1620-1622.

Naumoff, D. G., **2007**. Structure and evolution of the mammalian maltase-glucoamylase and sucrase-isomaltase genes. *Molecular Biology*, 41 (6): pp. 962-973.

Nichols, B. L., Avery, S., Sen, P., Swallow, D. M., Hahn, D., and Sterchi, E. E. **2003**. The maltase-glucoamylase gene: common ancestry to sucrase-isomaltase with complementary starch digestion activities. *PNAS*, 100(3): pp. 1432-1437.

Nichols, B., Quezada-Calvillo, R., Robayo-Torres, C., Ao, Z., Hamaker, B., Butte, N., Marini, J., Jahoor, F., and Sterchi, E. **2009**. Mucosal maltase-glucoamylase plays a crucial role in starch digestion and prandial glucose homeostasis of mice. *Journal of Nutrition*, 139(4): pp. 684-690.

Oizumi, T., Daimon, M., Jimbu, Y., Kameda, W., Arawaka, N., Yamaguchi, H., Ohnuma, H., Sasaki, H., and Kato, T. **2007**. A palatinose-based balanced formula improves glucose tolerance, serum free fatty acid levels and body fat composition. *Tohoku Journal of Experimental Medicine*, 212(2): pp. 91-99.

Ozaki, S., Oe, H., and Kitamura, S. **2008**. Alpha-glucosidase inhibitor from Kothala-himbutu (*Salacia reticulata* WIGHT). *Journal of Natural Products*, 71(6): pp. 981-984.

Purich, D. **1983**. Contemporary enzyme kinetics and mechanism: Selected methods in enzymology. New York: *Academic Press, Inc.*: Chapter 10.

Quezada-Calvillo, R., Robayo-Torres, C., Opekun, A., Sen, P., Ao, Z., Hamaker, B. R., Quaroni, A., Brayer, G. D., Wattler, S., Nehls, M. C., Sterchi, E. E., and Nichols, B. L. **2007**. Contribution of mucosal maltase-glucoamylase activities to mouse small intestinal starch alpha-glucogenesis. *Journal of Nutrition*, 137(7): pp. 1725-1733.

Quezada-Calvillo, R., Robaya-Torres, C., Ao, Z., Hamaker, B., Quaroni, A., Brayer, G., Sterchi, E. E., Baker, S., and Nichols, B. L. **2007**. Luminal substrate "brake" on mucosal maltase-glucoamylase activity regulates total rate of starch digestion to glucose. *Journal of Pediatric Gastroenterology and Nutrition*, 45: pp. 32-43.

Quezada-Calvillo, R., Sim, L., A., Zihua, Hamaker, B. R., Quaroni, A., Brayer, G. D., Sterchi, E. E., Robayo-Torres, C. C., Rose, D. R., and Nichols, B. L. **2008**. Luminal starch substrate "brake" on maltase-glucoamylase activity is located within the glucoamylase subunit. *Journal of Nutrition*, 138: pp. 685-692.

Reed, M., Lieb, A., and Nijhout, H. **2010**. The biological significance of substrate inhibition: a mechanism with diverse functions. *Bioessays*, 32(5): pp. 422-429.

Ren, L., Cao, X., Geng, P., Bai, F., and Bai, G. **2011**. Study of the inhibition of two human MGAM catalytic domains. *Carbohydrate Research*, 346: pp. 2688-2692.

Ren, L., Qin, X., Cao, X., Wang, L., Bai, F., Bai, G., Shen, Y. **2011**. Structural insight into substrate specificity of human intestinal maltase-glucoamylase. *Protein & Cell*, 2(10): pp. 827-836.

Rye, C. S. and Withers, S. G. **2000**. Glycosidase mechanisms. *Current Opinion in Chemical Biology*, 4: pp. 573-580.

Rossi, E. J., Sim, L., Kuntz, D., Hahn, D., Johnston, B. D., Ghavami, A., Szczepina, M. G., Kumar, N. S., Sterchi, E. E., Nichols, B. L., Pinto, B. M., and Rose, D. R. R. **2006**. Inhibition of recombinant human maltase glucoamylase by salacinol and derivatives. *FEBS Journal*, 273: pp. 2673-2683.

Rule, C. J., Wurzburg, B. A., and Ganem, B. **1985**. 3R, 4R-dixydroxy-L-proline: A potent and specific β-glucuronidase inhibitor. *Tetrahedron Letters*, 26(44): pp. 5379-5380.

Scofield, A. M., Fellows., L. E., Nash, R. J., and Fleet, G. W. J. **1986**. Inhibition of mammalian digestive disaccharidases by polyhydroxy alkaloids. *Journal of Life Sciences*, 39: pp. 645-650.

Segel, I. H. **1975**. Enzyme kinetics: Behavior and analysis of rapid equilibrium and stead-state enzyme systems. New York: *John Wiley & Sons*. Chapters 1-4.

Semenza, G. **1986**. Anchoring and biosynthesis of stalked brush border membrane proteins: Glycosidases and peptidases of enterocytes and renal tubuli. *Annual Review of Cell and Developmental Biology*, 2: pp. 255-313.

Serasinghe, S., Serasinghe, P., Yamazaki, H., Nishiguchi, K., Hombhanje, F., Nakanishi, S., Sawa, K., Hattori, M., and Namba, T. **1990**. Oral hypoglycemic effect of *Salacia reticulata* in the streptozotocin induced diabetic rat. *Phytotherapy Research*, 4(5): pp. 205-206.

Sim, L. **2010**. Structural and inhibition studies of human intestinal glucosidases. Ph.D. Thesis. University of Toronto: Canada.

Sim, L., Jayakanthan, K., Mohan, S., Nasi, R., Johnston, B. D., Pinto, B. M., and Rose, D. R. R. **2010**. New glucosidase inhibitors from an Ayurvedic herbal treatment for Type 2 Diabetes: Structures and inhibition of human intestinal maltase-glucoamylase with compounds from *Salacia reticulata*. *Biochemistry*, 49(3): pp. 443-451.

Sim, L., Quezada-Calvillo, R., Sterchi, E. E., Nichols, B. L., and Rose, D. R. **2008**. Human intestinal maltase-glucoamylase: crystal structure of the N-terminal catalytic subunit and basis of inhibition and substrate specificity. *Journal of Molecular Biology*, 375: pp. 782-792.

Sim, L., Willemsma, C., Mohan, S., Naim, H. Y., Pinto, B. M., and Rose, D. R. **2010**. Structural basis for substrate selectivity in human maltase-glucoamylase and sucrose-isomaltase N-terminal domains. *Journal of Biological Chemistry*, 285(23): pp.17763-17770.

Sinnott, M. **2007**. Carbohydrate chemistry and biochemistry: Structure and mechanism. Cambridge, United Kingdom: *The Royal Society of Chemistry*. Chapter 5.

Stein, R. L. **2011**. Kinetics of enzyme action: Essential principles for drug hunters. Hoboken; New Jersey*: John Wiley & Sons*. pp. 24-28.

Stütz, A. E. **1999**. Iminosugars as glycosidase inhibitors: Nojirimycin and beyond. Weinheim; New York: *Wiley-VCH*. Chapter 3.

Tanabe, G., Matsuoka, K., Yoshinaga, M., Xie, W., Tsutsui, N., Amer, M., Nakamura, S., Nakanishi, I., Wu, X., Yoshikawa, M., and Muraoka, O. **2012**. Role of the side chain stereochemistry in the α-glucosidase inhibitory activity of kotalanol, a potent natural α-glucosidase inhibitor. Part 2. *Bioorganic & Medicinal Chemistry*, 20: pp. 6321-6334.

Truscheit, E., Frommer, W., Junge, B., Muller, L., Schmidt, S. S., and Wingender, W. **1981**. Chemistry and biochemistry of microbial α-glucosidase inhibitors. *Angewandte Chemie International Edition*, 20: pp. 744-761.

van de Laar, F. A., Lucassen, P. L., Akkermans, R. P., van de Lisdonk, E. H., Rutten, G. E., and van Weel, C. **2005**. α-glucosidase inhibitors for patients with type 2 diabetes: Results from a Cochrane systematic review and meta-analysis. *Diabetes Care*, 28(1): pp. 154-163.

West, L. F., Davis, M. B., Green, F. R., Lindenbaum, R. H., and Swallow, D. M. **1988**. Regional assignment of the gene coding for human sucrase-isomaltase (SI) to chromosome 3q25-26. *Annals of Human Genetics*, 52: pp. 57-61.

Whitely, C. G. **1997**. Enzyme kinetics: Partial and complete competitive inhibition. *Biochemical Education*, 25(3): pp. 144-146.

Yoshikawa, M., Morikawa, T., Matsuda, H., Tanabe, G., and Muraoka, O. **2002**. Absolute stereostructure of potent α-glucosidase inhibitor, salacinol, with unique thiosugar sulfonium sulfate inner salt structure from *Salacia reticulata*. *Bioorganic & Medicinal Chemistry*, 10: pp. 1547-1554.

Yoshikawa, M., Murakami, T., Shimada, H., Matsuda, H., Yamahara, J., Tanabe, G., and Muraoka, O. **1997**. Salacinol, potent antidiabetic principle with unique thiosugar sulfonium sulfate structure from the Ayurvedic traditional medicine *Salacia reticulate* in Sri Lanka and India. *Tetrahedron Letters*, 38(48): pp. 8367-8370.

Yoshikawa, M., Murakami, T., Yashiro, K., and Matsuda, H. **1998**. Kotalanol, a potent alpha-glucosidase inhibitor with thiosugar sulfonium sulfate structure, from antidiabetic Ayurvedic medicine *Salacia reticulata*. *Chemical & Pharmaceutical Bulletin (Tokyo)*, 46(8): pp. 1339-1340.

Yoshikawa, M., Xu, F., Nakamura, S., Wang, T., Matsuda, H., Tanabe, G., and Muraoka, O. **2008**. Salaprinol and ponkoranol with thiosugar sulfonium sulfate structure from *Salacia prinoides* and alpha-glucosidase inhibitory activity of ponkoranol and kotalanol desulfate. *Heterocycles*, 75(6): pp. 1397-1405.

Yuasa, H., Takada, J., and Hashimoto, H. **2001**. Glycosidase inhibition by cyclic sulfonium compounds. *Bioorganic & Medicinal Chemistry Letters*, 11: pp. 1137-1139.

Appendix I

Documentation of a Ct-MGAM N2 nickel column purification, performed as described in the Materials and Methods, is included in Figures 39, 40, and 41.

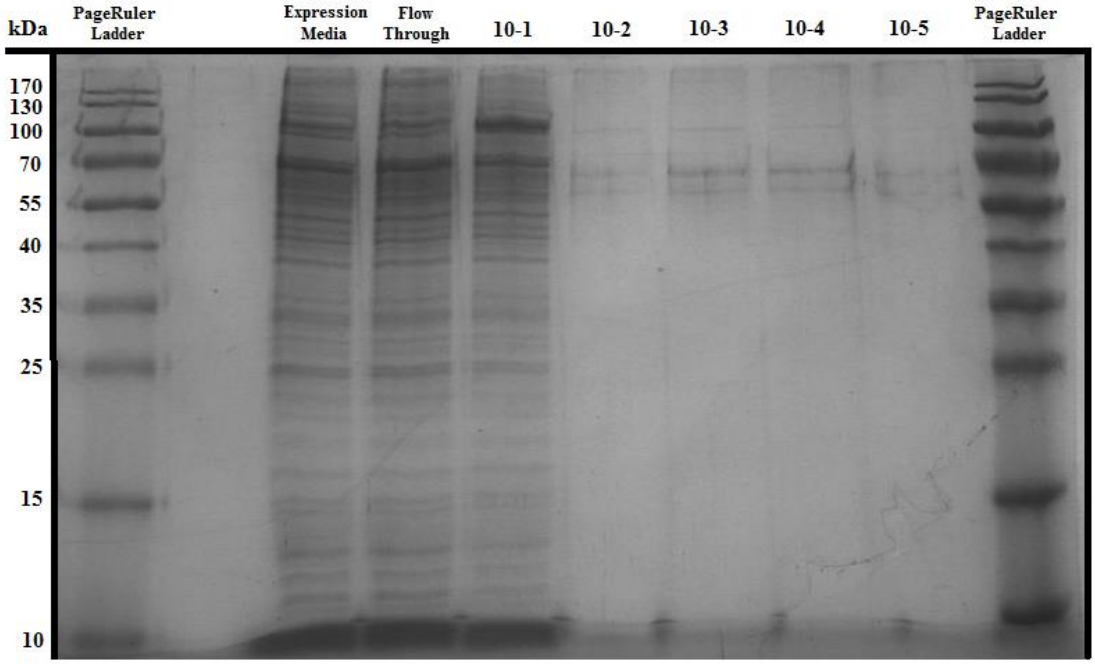

Figure 39. Ct-MGAM N2 purification: Expression media, flow through, and 10 mM imidazole elutions (14% denaturing gel).

Numbered gel columns indicate both the concentration of imidazole used to elute the proteins in each sample and the order of elutions (*ex.* 10-1 is the first elution of a series using a buffer with 10 mM imidazole).

Figure 40 contains a photo of another reducing gel showing elutions from this purification.

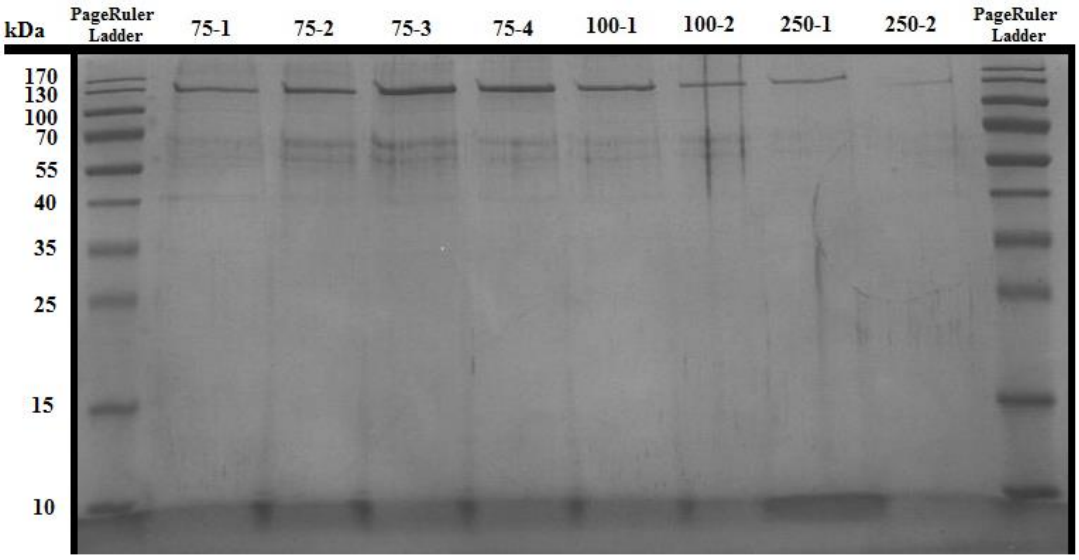

Figure 40. Ct-MGAM N2 purification: 75 – 250 mM imidazole elutions (14% denaturing gel).

Final purified proteins from the Ct-MGAM N2 purification are shown in Figure 41. Ct-MGAM N2 from the first column (75-250: Ct-MGAM N2) was used in assay for inhibition of PNP-glucose hydrolysis by DAB-1.

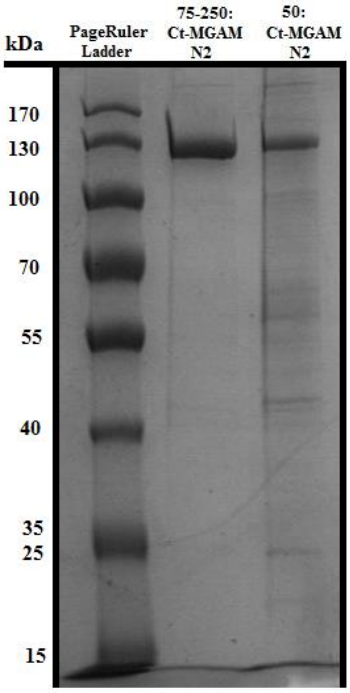

Figure 41. Ct-MGAM N2 purification: final preparations after protein concentration (10% denaturing gel).